Geochimica et Cosmochimica Acta 388 (2025) 268–282

Contents lists available at ScienceDirect

Geochimica et Cosmochimica Acta

journal homepage: www.elsevier.com/locate/gca

Foraminiferal denitrification and deep bioirrigation influence benthic biogeochemical cycling in a seasonally hypoxic fjord

Subhadeep Rakshit [a,*], Nicolaas Glock [b], Andrew W. Dale [c], Maria M.L. Armstrong [a], Florian Scholz [b], Andrè Mutzberg [c], Christopher K. Algar [a]

[a] Department of Oceanography, Dalhousie University, Halifax, Nova Scotia, Canada
[b] Institute for Geology, University of Hamburg, Bundesstraße 55, 20146 Hamburg, Germany
[c] GEOMAR Helmholtz Centre for Ocean Research Kiel, Kiel, Germany

ARTICLE INFO

Associate editor: Christof Meile

Keywords:
Sediment early diagenesis
Foraminiferal denitrification
Tubeworm
Benthic flux
Reaction transport modeling

ABSTRACT

Benthic macro- and micro-biota often play significant roles in controlling the biogeochemical dynamics in sediments. Their activity can be influenced by oxygen availability and impacted by the rise in global hypoxia in coastal regions over the last decades. To understand how these organisms interact with coastal hypoxia and influence sediment biogeochemistry, we undertook a study of early diagenesis in Bedford Basin, a seasonally hypoxic fjord on the West Atlantic coast in Nova Scotia, Canada, using a combination of observations and reaction-transport modeling. We observed that the seafloor was a source of ammonium and sink of nitrate with average fluxes of 2.2 ± 1.8 and −0.9 ± 0.7 mmol m^{-2} d^{-1} respectively. The diffusive oxygen uptake was 14 ± 4.6 mmol m^{-2} d^{-1} and the total organic carbon content in collected sediment cores was 5–7 % with a C/N ratio of ~10. The pyrite content increased steadily from 0.5 wt% Fe at surface to ~2 wt% Fe at 20 cm depth. Hydrogen sulfide was negligible down to 25 cm depth most of the time. The sediment was inhabited by tube-forming polychaete *Spiochaetopterus* sp. that formed tubes up to ~30 cm in length. The living foraminiferal assemblage in the top 5 cm sediment was found to be dominated (>85 %) by nitrate-storing and denitrifying benthic foraminifera *Stainforthia fusiformis*. These observations were used to develop and constrain a biogeochemical reaction-transport model. The model results suggest that the observed decrease in porewater concentrations of ammonium and dissolved inorganic carbon below 5 cm depth, was due to deep bioirrigation by tubeworms, accounting for almost 50 % of the benthic efflux. The model further revealed that the deep bioirrigation along with bioturbation and iron cycling prevented accumulation of free sulfide in the top 25 cm sediment despite oxygen penetration depths of ~1 mm. Modelled organic carbon and nitrogen deposition was 25.2 and 2.9 mmol m^{-2} d^{-1} with burial efficiencies of 23 % and 17 %, respectively. The model indicated a total denitrification rate of 1.3 mmol N m^{-2} d^{-1} that was largely (~70 %) driven by benthic foraminifera. This study reports the first evidence of foraminiferal denitrification in western Atlantic coastal sediments, and suggests that eukaryote mediated denitrification is an important driver of sediment N-loss in seasonally hypoxic environments, a process that has been traditionally assumed to be carried out by prokaryotic microbes.

1. Introduction

Coastal oceans are amongst the most productive regions of the planet, driven by the high nutrient input from land due to both natural and anthropogenic sources (Field et al., 1998). The organic matter synthesized there is subsequently remineralized in the water column and sediment, consuming oxygen and releasing inorganic nutrients that can be re-utilized by autotrophs. Due to a relatively shallow water column, coastal and shelf sediments receive a large portion of the sinking organic matter and its subsequent degradation drives a cascade of redox sensitive reactions (Jahnke et al., 1990). Regenerated nutrients can be returned to the water column, stored in the sediment or, in the case of nitrogen, removed from the ecosystem through denitrification. Coastal and shelf sediments account for more than half of the total N loss from the marine system (Middelburg et al., 1996; Bohlen et al., 2012).

Denitrification coupled to organic matter degradation using nitrate

* Corresponding author at: Atmospheric and Oceanic Sciences, Princeton University, Princeton, NJ, USA.
E-mail address: subhadeep.rakshit@dal.ca (S. Rakshit).

https://doi.org/10.1016/j.gca.2024.10.010
Received 8 May 2024; Accepted 10 October 2024
Available online 14 October 2024

as the terminal electron acceptor is usually referred to as canonical denitrification and generally assumed to be mediated by prokaryotic bacteria. However, this conception has been challenged with the discovery of certain benthic foraminifera (unicellular eukaryotes) that can store nitrate intra-cellularly at high concentrations and are capable of performing complete denitrification (Risgaard-Petersen et al., 2006). Since the discovery of denitrifying foraminifera in a hypoxic Swedish fjord, they have been identified in various places and accounted for 2–100 % of total denitrification in the sediments where they have been observed (Piña-Ochoa et al., 2010; Glock et al., 2013; Choquel et al., 2021; This study). Bioavailable N can also be removed by some chemoautotrophic bacteria performing anammox, where ammonium is oxidized to N_2 gas by nitrite. This process can account for up to 10 % of total N_2 production in estuarine sediment (Burdige, 2011). While denitrification and anammox remove bioavailable nitrogen, dissimilatory nitrate reduction to ammonium (DNRA) by some bacteria retains bioavailable N in the ecosystem (Giblin et al., 2013; Hardison et al., 2015).

The degradation of organic matter in sediments also plays a crucial role in the C, O, N, Mn, Fe, and S cycles (Berner, 1980). Terminal electron acceptors are used as oxidants for organic matter oxidation in the following sequence according to their Gibbs free energy yield; $O_2 > NO_3^- >$ Mn-oxides > Fe-oxides > $SO_4^{2-} > CH_2O$ (Tromp et al., 1995). In organic rich sediments, such as in coastal and estuarine sediments, oxygen is consumed within the top few millimetres, and numerous other tightly coupled redox-sensitive reactions occur in short succession within the uppermost centimeters (Seitaj et al., 2017). Reaction-transport models have been used to simulate benthic fluxes along with the rates and mechanisms of coupled reactions (Boudreau, 1997; Soetaert et al., 2000; Lessin et al., 2018). These models can also be useful in testing hypotheses and understanding the benthic response to changes in the environment.

In this study, we focus on Bedford Basin (BB) (Fig. 1), a semi-enclosed estuarine fjord on the coast of the Northwest Atlantic. It is 70 m deep and connected to the Scotian Shelf through a 20 m deep sill that restricts circulation in the water masses below the sill depth (Petrie and Yeats, 1990; Shan et al., 2011). The bottom water of BB is usually oxygenated every year due to winter mixing and infrequently in summer-fall due to shelf water intrusions (Rakshit et al., 2023). It is a eutrophic basin, where a distinct phytoplankton bloom occurs in spring and fall. Primary productivity is usually sustained throughout the year except in winter via supply of nutrients from sewage outfalls, the Sackville River, or from basin bottom water and sediments. During stratified periods, oxygen consumption in the bottom water and sediments leads to the onset of hypoxic conditions in late summer and fall. This seasonality makes BB a "natural laboratory" to study the development of coastal hypoxia and the corresponding biogeochemical impacts on the coupled cycles of carbon, oxygen, and nitrogen. In addition, a long-term weekly time-series station for oceanographic monitoring has been maintained there by the Bedford Institute of Oceanography (BIO) since 1992 (Li et al., 1998, 2010; Li and Harrison, 2008). Further, BB bottom water features annual nitrification cycles that have been studied recently (Haas et al., 2021, 2022). Although many oceanographic aspects have been documented, the coupled benthic-pelagic oxygen and nutrient cycles in BB have yet to be investigated in detail.

The sediments below 30 m water depth are dominated by silty clay and are rich in organic matter (Fader and Miller, 2008). Underwater camera surveys revealed that the seafloor is inhabited by long tube-worms (*Spiochaetopterus* spp.) (Hargrave, 1989; Fader and Miller, 2008). Some patches of bacterial mats, probably *Beggiatoa* spp., have also been identified (Fader and Miller, 2008). Scott (2005) studied the distribution of benthic foraminifera in BB and reported the presence *Fursenkoina fusiformis* (*Stainforthia fusiformis* according to Hayward et al., (2023)) in the deep basin. Certain unidentified foraminifera species from the genus *Stainforthia* have been shown to denitrify (Piña-Ochoa et al., 2010). Although denitrification rates of *S. fusiformis* have not been specifically measured, this species clusters in the phylogenetic tree with other denitrifying foraminifera (Woehle et al., 2022). Their existence in BB raises immediate curiosity in understanding their role in benthic nutrient cycling and adds to the motivation for this study. Hence, we measured the sediment–water fluxes and concentrations of nutrients and solids in BB sediment. Additionally, we performed sediment incubations

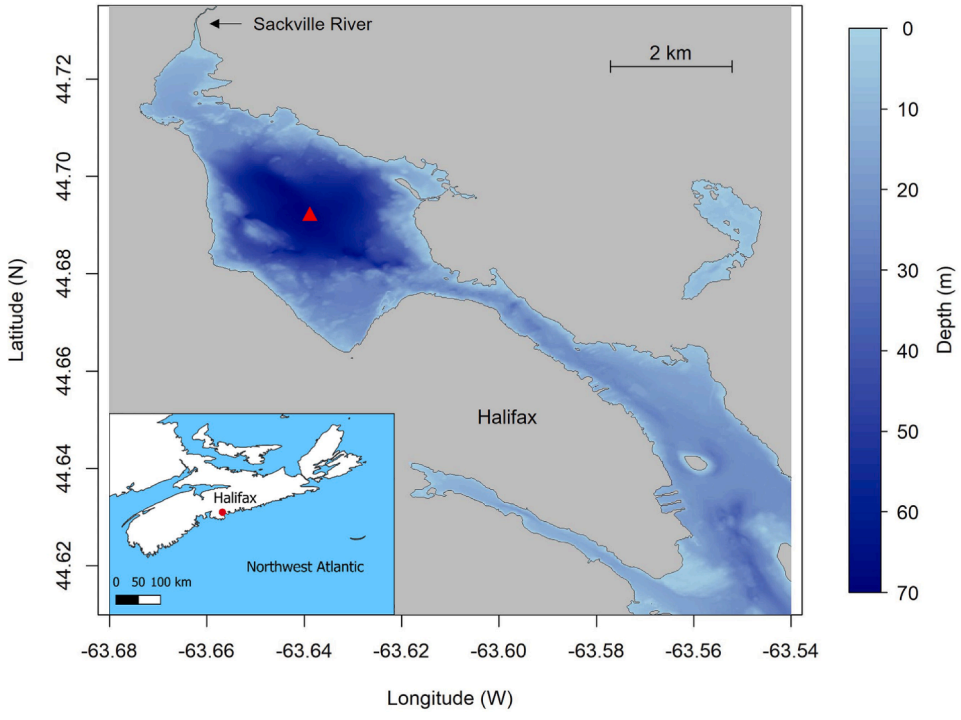

Fig. 1. Bathymetric map of Bedford Basin and Halifax Harbour. The red triangle indicates the Compass Buoy site. The inset shows its location in Nova Scotia adjacent to the city of Halifax.

to determine how the organic carbon remineralization rate changes with depth. We also quantified the abundance of living *S. fusiformis* and measured intracellular nitrate storage to assess its role in benthic N-cycling in BB. We used these data to constrain a reaction-transport model to identify the major early diagenetic processes involving C, N, O, Fe, and S cycling in BB sediment.

2. Materials and method

2.1. Study area and sampling

Sediment cores were collected from BB Compass Buoy station (Lat: 44.6937°N, Lon: 63.6403°W) using a multi-corer (KC Denmark) in February, May, August, November 2019, November 2020, May and November 2021, and March 2022 (Table 1). The core barrels were 60 cm long with 10 cm internal diameter, made of polycarbonate, and each recovered approx. 35 cm of sediment and 25 cm of water whilst keeping the sediment–water interface intact. Recovered cores were transported on ice to a temperature-controlled lab (~4 °C) within 3 h of collection. From November 2020 onwards, the cores were submerged immediately after recovery into larger core barrels filled with bottom water to minimize oxygen contamination during transportation. The number of cores collected each day varied from 8 to 12. Depending upon the number of cores collected, duplicate or triplicate cores were used to extract porewater using Rhizon samplers (0.2 μm pore size) at 2 cm intervals, and/or sectioning and centrifuging for 15 min at 5000 rpm. For the latter case, the supernatant was filtered through a 0.45 μm cellulose acetate filter. Porewater was analyzed for ammonium (NH_4^+), nitrate + nitrite, ferrous iron (II) (Fe^{2+}), and hydrogen sulfide (H_2S). From November 2020 onwards, dissolved inorganic carbon (DIC) was also measured. Ammonium (Solórzano, 1969), hydrogen sulfide (Cline, 1969) and Fe (II) (Viollier et al., 2000) were measured spectrophotometrically. Nitrite + nitrate (hereafter approximated as nitrate) was measured using a chemiluminescence method (Hendrix and Braman, 1995) with a Thermalox-NOx instrument. DIC was measured using an Apollo SciTech DIC analyzer, and calibrated with certified reference material (Scripps Institution of Oceanography). The precision of the method was 0.4 %. One core from each sampling date was extruded upwards until 6 cm of overlying water remained, after which two to five oxygen profiles were recorded using Unisense™ microelectrodes at 100 μm vertical resolution (Rakshit et al., 2023). The diffusive oxygen uptake (DOU) was calculated from these oxygen profiles by fitting a 1D steady state reaction-transport model of sediment oxygen consumption (Rakshit et al., 2023). Duplicate or triplicate cores were used for determining benthic nutrient fluxes ex-situ by whole core incubation (see below). Nutrient concentrations in overlying bottom water samples were measured using an autoanalyzer (Skalar San++ autoanalyzer) following standard laboratory protocols (McGrath et al., 2019). For November 2020 and May 2021, one core was sectioned to determine vertical carbon remineralization rates as described below.

For sampling events in 2019, one sediment core was sectioned in 1–2 cm intervals. Porosity was measured in these samples by taking the wet and dry weight of the sediment, assuming a dry sediment density of 2.65 g cm^{-3} and a mean measured salinity of 31. Porosity variation with depth was described by the equation,

$$\varphi = \varphi_{inf} + (\varphi_0 - \varphi_{inf}) e^{-\frac{z}{\varphi_{att}}} \quad (1)$$

here φ is porosity at depth z, φ_0 and φ_{inf} is porosity at surface and in compacted sediment, respectively, and φ_{att} is the porosity attenuation. The sectioned sediment was also used to determine total carbon and total nitrogen using an elemental analyzer (Costech ECS4010). A previous study (Black et al., 2023) did not find any significant difference in carbon content between acid fumigated (5.5 % ± 0.5%, n = 29) and non-fumigated (5.7 % ± 0.8%, n = 39) samples, indicating the total carbon in BB sediment is representative of total organic carbon (TOC). Additionally, dried sediment samples were analyzed for excess ^{210}Pb for determining the sedimentation and bioturbation rate (Black et al., 2023). In May 2019, dried sediments were also analyzed for operationally defined solid iron pools following the sequential extraction scheme of Poulton and Canfield (2005). In brief, Fe bound to carbonate minerals was extracted with sodium acetate, Fe bound to (oxyhydr) oxide minerals was extracted with sodium dithionite and magnetite Fe was extracted with ammonium oxalate. Note that the actual minerals recovered by this method may differ from the operational definition (Slotznick et al., 2020; Hepburn et al., 2020; Retschko et al., 2023). Extraction solutions were analyzed for Fe concentration by ICP-OES. Concentrations of Fe bound as pyrite were determined by the chromium reduction method (Canfield et al., 1986). The sum of sequentially extracted Fe fractions and pyrite-Fe is referred to as reactive Fe in this study. For the purpose of this study, particulate iron depth profiles were assumed to be invariable across seasons since these analyses were not repeated on other sampling dates.

2.2. Whole core incubations

For ex-situ whole core incubations, duplicate or triplicate cores were kept in a cold room (~4 ℃). Core tops were fitted with caps as airtight as

Table 1
Sampling dates, corresponding bottom water conditions (60 m depth) and fluxes determined ex situ. Uncertainties on fluxes correspond to multiple measurements (duplicate or triplicate core incubations). Uncertainties on DOU are calculated from multiple microsensor profiles. Negative sign implies the direction of the flux is from the bottom water into the sediment, and vice versa.

Sampling date	BW temp ℃	BW salinity	BW O_2 μM	BW NH_4^+ μM	BW NO_3^- μM	DOU flux mmol m^{-2} d^{-1}	DIC flux mmol m^{-2} d^{-1}	NH_4^+ flux mmol m^{-2} d^{-1}	NO_3^- flux mmol m^{-2} d^{-1}
12-Feb-2019 †2	4.9	31.39	144	1.0	9.5	−15.5 ± 5.7 (n = 3)	n/a	1.4 ± 0.1	−1.20 ± 0.01
07-May-2019 †2	1.1	31.03	292	3.7	4.6	−20.9 ± 0.5 (n = 2)	n/a	0.6	−0.27
26-Aug-2019 †3	1.5	30.97	94	16.6	6.9	−13.9 ± 5.1 (n = 2)	n/a	1.3 ± 0.4	−0.05 ± 0.17
07-Nov-2019 †3	2.0	30.93	32	16.8	13.5	−7.1 ± 1.7 (n = 2)	n/a	6	−2.0
04-Nov-2020 †3	5.1	31.67	186	1.6	12.5	−15.1 ± 1.3 (n = 3)	22.0 ± 8.5	2.3 ± 0.5	−0.80 ± 0.02
04-May-2021 †3	4	31.25	124	1.5	20.4	−11.5 ± 0.9 (n = 3)	3.8 ± 1.7	1.2 ± 0.1	−1.0 ± 0.1
02-Nov-2021 †3	4.3	31.06	3	5.2	18.4	n/a	21.1 ± 6.2	2.7 ± 0.2	−1.30 ± 0.04
Mean	3.3 ± 1.7	31.19 ± 0.27	125 ± 97	6.7 ± 7.0	12.3 ± 5.8	−14 ± 4.6	15.6 ± 10.2	2.2 ± 1.8	−0.9 ± 0.7
Model	4*	31*	170*	7.2*	12.2*	−13.2†	19.6	2.2	−1.1

* Imposed boundary condition to the model, determined from the Bedford Basin Monitoring Program. †Total oxygen flux. †2Two replicates were used for core incubation. †3Three replicates were used for core incubation.

possible. The caps were fitted with a magnetic stirrer to prevent the development of concentration gradients in the water column without disturbing the sediment surface. Additionally, the caps were fitted with a port for inserting an oxygen probe (Hach LDO probe), which recorded the oxygen concentration in the bottom water every 15 min (this data was not reported because in most cases it showed inconsistent oxygen drawdown, likely due to air leakage from core caps), as well as two ports for sampling the bottom water and a port for bubbling with gas. An air-N_2 gas mixture was bubbled for three hours to maintain the bottom water at *in-situ* oxygen level prior to beginning the incubations. The later port was then closed, and the core left to settle for two hours before beginning the experiment. The cores were incubated for 24 h, during which water samples were collected at four equally spaced time points (~8 h). The water samples were collected using a syringe from one sampling port, while the other sampling port was connected to a bottom water reservoir to replace the extracted water. The collected water samples were filtered (0.45 μm) and stored frozen at −20℃ until further analysis. The concentration data were used to determine benthic fluxes of ammonium and nitrate using the following equation:

$$Flux = dC/dt \times h \quad (2)$$

where dC/dt is the change in concentration of solute in the overlying water during the incubation and h is the height of the water. Fluxes are reported in mmol m^{-2} d^{-1}. Positive fluxes are out of sediment to the bottom water and negative fluxes are from the bottom water into the sediment.

From November 2020 onwards, a water sample was additionally collected at the beginning and at the end of the experiment to determine the DIC flux. These samples were collected in 12 ml Labco Exetainer glass vials, filled from the bottom, and overflowed to ensure that no air-bubbles were formed or trapped in the vials while sampling. Samples were fixed with 10 μl saturated $HgCl_2$, capped and stored at 4 ℃ without headspace until analysis. Additional samples were collected from the bottom water reservoir at the beginning and at the end of all the flux experiments and analyzed for any change in concentration. No attempt was made to prevent air contact in the bottom water reservoir other than keeping the lid closed.

2.3. Anoxic sediment incubations

Anoxic incubations were used to determine organic carbon remineralization rates vertically through the sediment. Sediment cores were sliced at 0–2, 2–4, 8–10, 16–18 cm intervals into Ziploc bags, and then the samples were immediately transferred to a N_2-filled glove box to minimize oxygen exposure. Inside the glove box, samples were homogenized within the bag. A small cut was made on the bottom corner of the Ziploc bag and the sediment was squeezed into eight 15 ml centrifuge tubes leaving no headspace. The caps were further wrapped with parafilm. Four bottles of 1000 ml ascorbic acid solution (i.e., anoxic solution) (1000 ml MQ water + 20 g sodium ascorbate + 4 g NaOH) were prepared. The tubes were then submerged in the solution and incubated in darkness at *in-situ* (4 °C) temperature to maintain anoxia within the tubes. Two sediment tubes from each depth were removed and sampled at the beginning, and then after 1, 3 and 7 weeks. The dissolved oxygen concentration of the bottled ascorbic acid was measured during sampling with a handheld Hach LDO probe. It was consistently <1 % air saturation. Sampled tubes were centrifuged at 5000 rpm for 15 min. The tubes were opened inside a glove box under N_2 atmosphere and the extracted porewater was filtered (0.45 μm) and analyzed for DIC, NH_4^+, Fe^{2+}, H_2S.

The sedimentary organic carbon remineralization rate was determined from the production of DIC over time. Similarly, organic nitrogen remineralization (ammonification) was also determined from the production of NH_4^+ after accounting for the adsorption on particle as

$$NH^+_{4total} = NH^+_{4pw}\{\varphi + (1-\varphi)\rho_s K_{ads}\} \quad (3)$$

where NH^+_{4total} and NH^+_{4pw} are total and porewater NH_4^+ concentration, respectively, φ is porosity, ρ_s is dry sediment density and K_{ads} (=1.6 cm^3 g^{-1}) is the adsorption coefficient (Berg et al., 2003). Not considering adsorption could lead to an underestimation of ammonification by ~20 %. The calculation assumes that nitrification or anammox rates were zero, which is reasonable since the incubations were conducted under anoxic conditions.

2.4. Sampling for foraminifera

In November 2020 and May 2021, one core was sectioned at 1 cm intervals over the top 5 cm and collected in 500 ml glass jars. Rose Bengal was added to stain the cytoplasm of living foraminifera. Rose Bengal (2 g) was dissolved in 1 L ethanol in a separate conical flask, from which 200 ml was added to each glass jar to provide a sediment − ethanol slurry of 30%/70% v/v. The slurry was gently stirred and uniformly mixed. The jars were capped and wrapped with parafilm. The height of the sediment slurry in each jar was marked with ink for later determination of the sediment volume (next section) and the jars were stored (>2 weeks) at room temperature until further analysis. Additionally, in March 2022 we performed benthic foraminiferal sampling with the aim of recovering live foraminifera samples to determine their intra-cellular nitrate content.

2.4.1. Determination of living abundances

The samples stained with Rose Bengal were wet sieved over a 125-μm and 63-μm mesh. The >125-μm and the 63–125-μm fractions were collected separately and dried at ~40 °C. Afterwards, the sample jars were filled with water up to the slurry fill mark level. The volume of the water representing the bulk sediment volume + 200 ml ethanol/Rose Bengal was measured in a graduate cylinder (accuracy ~ ± 5 cm^3). The slurry level mark on the sample jars of the top cm sample from November 2020 was not recognizable at the time of measurement and, thus, could not be determined. For the following analyzes we assumed the same sample volume as in the top cm from May 2021. Subsequently, samples were split and specimens of foraminifera that were stained with Rose Bengal were counted under the microscope. Living stained foraminifera were fixed in plummer cells. Living abundances were determined from the number of stained foraminifera and the bulk sediment volume.

2.4.2. Preparation of living specimens for intracellular nutrient analyses

To collect living foraminifera specimens for the intracellular NO_3^- analyses, samples from March 2022 were directly wet sieved within two days after sampling using filtered seawater from BB (these samples were not stained or put in ethanol solution). Three samples of 9 to 70 living *Stainforthia fusiformis* specimens and two additional samples of 8 and 11 living *Elphidium bartletti* specimens were picked since these were the most abundant benthic foraminifera species in the deep basin. All samples were photographed with a stereomicroscope camera for the later determination of foraminiferal biovolume. Afterwards, foraminifera were cleaned and the NO_3^- extracted following the methodology of Glock et al., (2020). Briefly, specimens were rinsed with NO_3^--free artificial seawater prepared from Red Sea salt. Subsequently, they were transferred into centrifuge tubes with a small amount of artificial seawater. Then, 3 ml of MQ water was added to the samples. Within the water, foraminiferal specimens were broken, using a clean pipette tip. A procedural blank was carried through the same procedure without foraminiferal specimens for blank corrections of the NO_3^- analyses (five blanks in total). All samples were frozen at – 20 °C for at least two hours and thawed afterwards. This procedure was repeated three times to destroy plasma membranes and release intra-cellular NO_3^- for the analyses (Burke et al., 1976; Dowgert and Steponkus, 1984). Subsequently,

samples were filtered through sterile 0.2 μm cellulose-acetate filters and stored frozen for later analysis of nitrate concentration.

2.4.3. Biovolume determination of living foraminifera

The total foraminiferal cell volume of each species was estimated following Geslin et al. (2011). We assumed that the internal test volume corresponds to 75 % of the total test volume and was completely filled with cytoplasm (Hannah et al., 1994). Methodology and equations for exact biovolume estimation for several benthic foraminifera species are given by de Freitas et al. (2021). Since neither *S. fusiformis* nor *E. bartletti* are listed in de Freitas et al. (2021) we used the best resembling geometric shape for the biovolume estimation (i.e., cone for *S. fusiformis* and prolate spheroid for *E. bartletti*).

2.5. Numerical model

A one-dimensional, steady state, reaction-transport model for Organic Matter DIAgenesis (OMDIA) was developed to simulate the benthic biogeochemical processes in BB. The OMDIA model is conceptually similar to previously developed models (Soetaert et al., 1996a; Wang and Van Cappellen, 1996; Boudreau, 1997; Bohlen et al., 2012; Dale et al., 2016). The model includes 12 solutes, namely O_2, DIC, NH_4^+, NO_3^-, Fe^{2+}, Mn^{2+}, SO_4^{2-}, H_2S, CH_4, and H_2 and intracellularly stored NO_3^- (in foraminifera cell, and other bacteria; NO_{3for}^- and NO_{3bac}^- respectively) (Table S1). We also considered 10 solid species including three pools of organic matter – highly, medium, and poorly reactive (OM1, OM2, OM3), three reactive pools of iron (III) (oxyhydr)oxides – highly, medium, and poorly reactive fraction ($Fe(OH)_3$, $Fe(OH)_{3.MR}$, $Fe(OH)_{3.LR}$ respectively), two pools of MnO_2 (MnO_2 and $MnO_{2.MR}$), iron monosulfide (FeS) and pyrite (FeS_2). Solutes were modeled in μmol cm^{-3} of porewater, and solid species were modelled in μmol cm^{-3} of dry sediment (expressed in wt% of dry sediment in the plots) (Table S1). The top 50 cm of sediment was simulated over 100 grid layers of increasing thickness with depth. The stoichiometric reaction network and rate expressions are described in Table S2, S3, S4 and the corresponding model parameters are given in Table S5. The modelled species were transported in the sediment column by advection and compaction due to sedimentation, molecular diffusion, faunal bioturbation and bioirrigation. The following equations were used to express the change in concentration of solutes (Eq. (4), solids (Eq. (5), and intracellular nitrate (Eq. (6):

$$\varphi\frac{\partial C_i}{\partial t}=\frac{\partial}{\partial z}(\varphi(D_b+D_s)\frac{\partial C_i}{\partial z})-\frac{\partial}{\partial z}(\varphi u C_i)+\varphi\alpha_i(C_{i(0)}-C_i)+\varphi\sum R_i \quad (4)$$

$$(1-\varphi)\frac{\partial C_j}{\partial t}=\frac{\partial}{\partial z}((1-\varphi)D_b\frac{\partial C_j}{\partial z})-\frac{\partial}{\partial z}((1-\varphi)vC_j)+(1-\varphi)\sum R_j \quad (5)$$

$$\varphi\frac{\partial C_{cNO3}}{\partial t}=\varphi\gamma(C_{cNO3(0)}-C_{cNO3})+\varphi\sum R_{cNO3} \quad (6)$$

where t is time, z is sediment depth, C_i and C_j represent concentration of solutes and solids respectively, and C_{cNO3} stands for intracellular nitrate stored in either benthic foraminifera or large bacteria. The nitrate uptake by these organisms can be assumed as non-local transport and therefore diffusive and advective transport terms are zero in Eq. (6). φ is porosity, and $(1-\varphi)$ is the solid volume fraction of the sediment. D_s is the tortuosity corrected diffusion coefficient for solutes after Boudreau (1996), $D_s = D_0/(1-2\ln(\varphi))$, where D_0 is the temperature and salinity corrected diffusion coefficient of the solute. u and v denote the advective velocity for solutes and solids, respectively. D_b is the bioturbation coefficient ($cm^2\ yr^{-1}$) determined from ^{210}Pb profiles (Figure S1). α_i ($year^{-1}$) is the bioirrigation coefficient and $C_{i(0)}$ is concentrations of solute in the bottom water. γ ($year^{-1}$) is a coefficient for non-local transport by foraminifera or other large vacuolated bacteria, and $C_{cNO3(0)}$ is the intracellular nitrate in equivalent pore water concentrations. In the model we assumed the intracellular nitrate storage was mainly due to foraminifera, where $C_{cNO3(0)}$ was determined as previously described. The bioirrigation coefficient for Fe^{2+} was set to 25% of the value of the other solutes due to its high tendency to be oxidized in presence of oxygen near the sediment water interface and in animal burrows (Dale et al., 2015). The non-local exchange processes were simulated using the equation,

$$\alpha = \alpha_{max}.\ (exp(\alpha_L - z))/(1+ exp(\alpha_L - z)) \quad (7)$$

$$\gamma = \gamma_{max}.\ (exp(\gamma_L - z))/(1+ exp(\gamma_L - z)) \quad (8)$$

Eq. (7) represents bioirrigation coefficient α, α_{max} is the maximum value of bioirrigation which is constant till the depth of α_L, beyond this depth the value exponentially decreases to zero. Similarly, equation 8 denotes foraminiferal nitrate transport coefficient γ, and the maximum transport rate of γ_{max} is constant till γ_L depth after which it rapidly attenuates to zero. The bioirrigation coefficient, α, was determined by fitting the model to the observed NH_4^+ and DIC depth profiles.

In the equations, $\sum R$ denotes the sum of all the coupled reactions involving the chemical species. The coupled biogeochemical reactions considered in the model (Table S2) are driven by organic matter (OM) degradation. OM was degraded sequentially by aerobic respiration, denitrification, manganese (IV) oxide reduction, iron (III) oxide reduction, sulfate reduction and methanogenesis according to Gibbs free energy yield during respiration via different electron acceptors ($O_2 > NO_3^- > MnO_2 > Fe(OH)_3 > SO_4^{2-} > CH_2O$) (Tromp et al., 1995). The organic matter degradation rates were modelled using Michaelis-Menten kinetics in which the preferable electron acceptor solely oxidizes OM until its concentration reaches a limiting concentration defined by half-saturation concentration. Additionally, another inhibition by foraminiferal denitrification was implemented on OM degradation by other terminal electron acceptors using the formulation $K_{s.for}/(K_{s.for} + NO_{3for}^-)$, where $K_{s.for}$ is the half saturation constant for denitrification by foraminifera. This formulation was used because it was assumed that foraminifera, being motile, have an advantage over non-motile bacteria, and can actively seek fresh organic matter and refill their intracellular nitrate storage from bottom water or surface sediment using their pseudopodial network, vacuoles, and pores. Their abundance in BB was distributed throughout the top 5 cm and it is reasonable to assume that they survive by performing denitrification using internally stored nitrate at these depths whereas bacterial respiration takes place alongside (see results and discussion). Degradation of one mole of organic matter produces rNC moles of NH_4^+, where rNC is the molar ratio of N:C in OM. Secondary redox reactions (Table S2) were expressed using bimolecular rate laws (Wang and Van Cappellen, 1996).

2.6. Boundary conditions and model constraints

Upper and lower boundary conditions for all species (Table S1, S5) are required to solve the differential equations. For solutes, the upper boundary was defined as fixed concentrations. These were obtained by averaging the weekly bottom water concentrations of ammonium, nitrate, and oxygen recorded at 60 m by the Bedford Basin Time Series (Li, 2014; Haas et al., 2021). The sulfate concentration was assumed to be 25 mM, consistent with a bottom water salinity of 31. Bottom water DIC was determined from Niskin bottles collected during sampling in this study. Hydrogen sulfide, dissolved iron and manganese were assumed to be absent in the bottom water. The upper boundary for solids was defined as fixed fluxes. The OM and iron oxide fluxes were constrained with the model (Table S1). Zero gradient boundary conditions were applied to all species at the lower boundary. The parameters related to bioturbation were determined from measured excess ^{210}Pb profile (Figure S1) (Black et al., 2023).

To constrain the model with observations, we first adjusted the deposition flux of the three pools of organic matter and their reactivity to simulate the observed DIC efflux, TOC% and measured carbon remineralization rates from the anoxic incubations. Then, the

bioirrigation coefficients were adjusted to obtain the observed porewater profiles of NH_4^+ and DIC. The iron oxide fluxes, reactivities and transformation to iron sulfide were then adjusted to obtain the best visible fit with the observed contents of reactive iron, pyrite as well as dissolved Fe^{2+} and H_2S. At this point, most of the observed depth profiles and benthic fluxes could be simulated, except the nitrate influx observed in the whole core incubation experiments. Therefore, non-local intracellular nitrate uptake by benthic microorganisms was considered in the model. We ruled out the possibility of nitrate uptake by large sulfur bacteria and subsequent DNRA because the NH_4^+ data could be simulated without it. Besides, no filamentous bacterial mats were observed on the recovered sediment cores. Therefore, we assigned the entire non-local intracellular transport of nitrate to foraminiferal uptake performing benthic denitrification by adjusting γ in Eq. (6).

A finite difference scheme and the method of lines were applied to solve the coupled differential equations. The model was constructed using R package "ReacTran" (Soetaert and Meysman, 2012), and was solved using R package "deSolve" (Soetaert et al., 2010). Since the main goal of using the modeling approach here is to gain mechanistic understanding of the dominant biogeochemical drivers of benthic biogeochemistry at BB, the model represents the long-term average rather than intra-annual dynamics. Therefore, rather than trying to fit individual field conditions, the model was run to steady state and was constrained with the measured seasonally averaged benthic fluxes, pore water and solid profiles, and OM remineralization rates.

3. Results

3.1. Sediment appearance

The sediment was very soft, with a surface porosity >0.95 and decreasing to 0.90 at the bottom of the sediment cores (~30 cm). The sediment surface appeared to have a thin (~1 cm) yellowish oxidized layer. On most occasions, there was an abundance of 2–4 mm long rice grain shaped particles in the uppermost 1–2 cm, which appeared to be fecal pellets (Figure S2). The sediment below the surface layer was black in color. A sulfide smell was seldom detected during sediment core handling and sectioning. Populations of the tubeworm Spio*chaetopterus* sp. were abundant during sampling, with long tubes in most sediment cores up to >30 cm length. On occasions, live worms were found in some tubes at depths >20 cm during core sectioning.

3.2. Sediment geochemistry

The surface TOC content was 5–7 wt% and decreased with depth. The C/N ratio of organic matter was ~10 (Fig. 2A,B). The total reactive iron fraction, i.e., the sum of reactive iron (oxyhydro)oxides and iron in pyrite, at the surface sediment was ~4 wt% and showed a marginal decrease with depth, whereas pyrite content increased with depth reaching ~2 wt% (Fig. 2C, Figure S3). Samples between 13–17 cm contained elevated concentrations of total reactive iron driven by increase in both (oxyhydr)oxides and pyrite (Fig. 2C, Figure S3). However, due to lack of temporal and spatial data, we could not conclude if this trend was widespread, or that the intermediate elevated concentration was due to spatial heterogeneity. In this study we assume the latter. The degree of pyritization (Fe_{py}: Fe_{rectv}) increased consistently with depth and remained below a value of 0.6 down throughout the core (Figure S3).

The oxygen penetration depth was consistently ~1 mm (Fig. 2D). The porewater concentrations of NH_4^+ and DIC increased with depth in all seasons until ~5 cm depth with some seasonal variability. With the exception of winter 2019, the concentrations decreased consistently below this depth to the bottom of the sediment cores. The maximum concentrations at ~5 cm measured in fall for NH_4^+ and DIC were 290 μM (μmol L^{-1}) and 5800 μM, respectively, with minimum concentrations at 5 cm in May of 150 and 3200 μM, respectively. At depth, no seasonality was detected and the average concentrations at ~25 cm were 120 μM and 3500 μM, respectively, for NH_4^+ and DIC. This reversal of concentration gradients will be referred to as an 'inverse pore water profile' (Fig. 2E,F; Figure S4).

Porewater H_2S concentrations were negligible down to 25 cm depth in most seasons except for winter 2019 (Fig. 2I; Figure S4). Dissolved iron was highest at the surface and then decreased with depth (Fig. 2H; Figure S4). The maximum measured Fe^{2+} concentration was ~200 μM at ~2 cm. NO_3^- concentrations in surface layers were generally (10–20 μM) close to the bottom water, although on occasions very high NO_3^- concentrations were observed within the top 5 cm of sediment, with a maximum measured concentration of >60 μM at 5 cm depth. This may have been released from foraminifera vacuoles during sample handling (Bernhard et al., 2012). In deeper layers NO_3^- concentrations were negligible (Fig. 2; Figure S4).

3.3. Benthic solute fluxes

The benthic fluxes determined in this study are summarized in Table 1 and Fig. 3. The diffusive oxygen uptake (DOU) calculated from the microsensor oxygen gradients was previously reported in Rakshit et al. (2023) and shown to be linearly correlated with bottom water oxygen concentration. The maximum DOU was measured in summer when the water was well oxygenated, and the lowest DOU was measured in fall when the bottom water was hypoxic. Seasonality in the DIC efflux could not be determined due to the limited number of measurements. However, the summer DIC efflux appeared to be lower than in fall. The sediment was a source of NH_4^+ year-round. Although a clear seasonality could not be identified, NH_4^+ efflux appeared to be highest in fall, and lowest in early summer. The NO_3^- flux was directed into the sediment in all seasons and the influx was highest in fall. BB sediment was a weak net source of DIN, except during the fall months (Table 1). On average, the mean DOU and benthic flux of DIC, NH_4^+ and NO_3^- was -14 ± 4.6, 15.6 ± 10.2, 2.2 ± 1.8, and -0.9 ± 0.7 mmol m^{-2} d^{-1} respectively. These yearly averaged fluxes were used to constrain the steady state model.

3.4. Anoxic incubations and organic matter remineralization rate

The carbon and nitrogen remineralization rates are summarized in Table 2 and Fig. 4. Both rates decreased with depth in the sediment. Some seasonality was noticed in the surface layers (0–4 cm) but was less evident with depth (Table 2). The remineralization rate was higher in fall compared to early summer. The C/N ratio of remineralization was generally close to Redfield with no clear depth-trend (Table 2). During the incubations, a linear increase in Fe^{2+} concentration was noticed at depths 0–2 and 2–4 cm, but not for 8–10 and 16–18 cm sediment, indicating that dissimilatory iron reduction plays a more important role in organic matter remineralization in the top 4 cm (Figure S5, S6). Interestingly, the linear increase of Fe^{2+} stopped after 25 and 10 days of incubation in fall and early summer, respectively, and remained constant or decreased partially through the remaining duration of incubation. H_2S did not accumulate in the upper 4 cm for the entire duration of the incubation in fall, and only accumulated at the final sampling point in summer. However, at 8–10 cm and 16–18 cm, H_2S concentration increased with time in both seasons (Figure S5, S6).

3.5. Foraminifera abundances and intracellular nitrate content

Living foraminiferal abundances in the top 5 cm of the sediment varied from 234 ind. cm^{-2} in May 2021 to 496 ind. cm^{-2} in November 2020 (Table 3, S6). The two most abundant species were *Stainforthia fusiformis* (between 86 and 96% of the total living assemblages, Fig. 5) and *Elphidium bartletti* (between 4 and 13%). Other living species that were present included *Eggerelloides advena*, *Spiroplectamina biformis*, *Globobulimina affinis* and *Labrospira crassimarga* yet accounted for only a minor part of the living assemblages (0.2–0.6 %). The intracellular NO_3^-

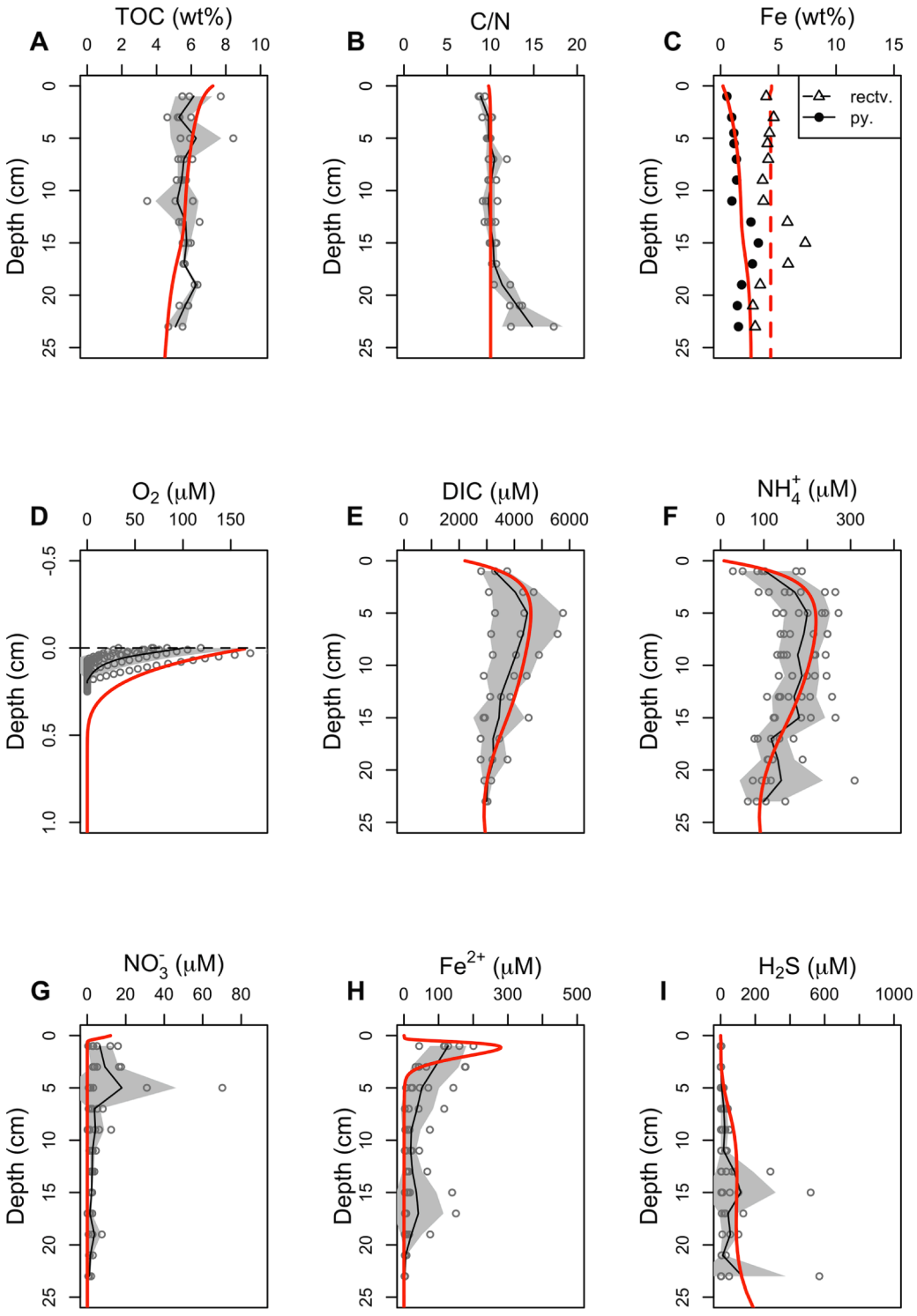

Fig. 2. (A-I) Sediment solid phase and porewater distributions in Bedford Basin. The symbols denote all the measured seasonal profiles. The black line denotes the seasonally averaged concentration. The gray area around the black line denotes the standard deviations (seasonal variation) of the mean. The red lines denote the steady state model simulation. The reactive iron in (C) represents the sum of iron (hydroxy)oxides and pyrite. Detailed seasonal trends can be seen in Figure S4.

concentration in *S. fusiformis* was 106.5 ± 43.0 mM (mmol L^{-1}) (n = 3), equivalent to 75.1 ± 23.8 pmol individual^{-1} (n = 3). *Elphidium bartletti* was found to have no notable NO_3^- storage.

3.6. Model results

The model generally simulated the seasonally averaged solid and porewater profiles, remineralization rates and benthic fluxes (Fig. 2,3,4). The depth integrated rates of the modeled reactions are shown in Table S2. The modeled deposition flux of organic carbon was 25.2 mmol m^{-2} d^{-1}, of which 19.6 mmol m^{-2} d^{-1} was remineralized and 5.6 mmol m^{-2} d^{-1} was buried, equal to a carbon burial efficiency of 23%. The model required the inclusion of deep bioirrigation (Figure S7) to correctly reproduce the inverse NH_4^+ and DIC porewater profiles (Fig. 2e, f). We attribute bioirrigation down to 30 cm mainly to the activity of long tubeworms due to their dominant presence in the

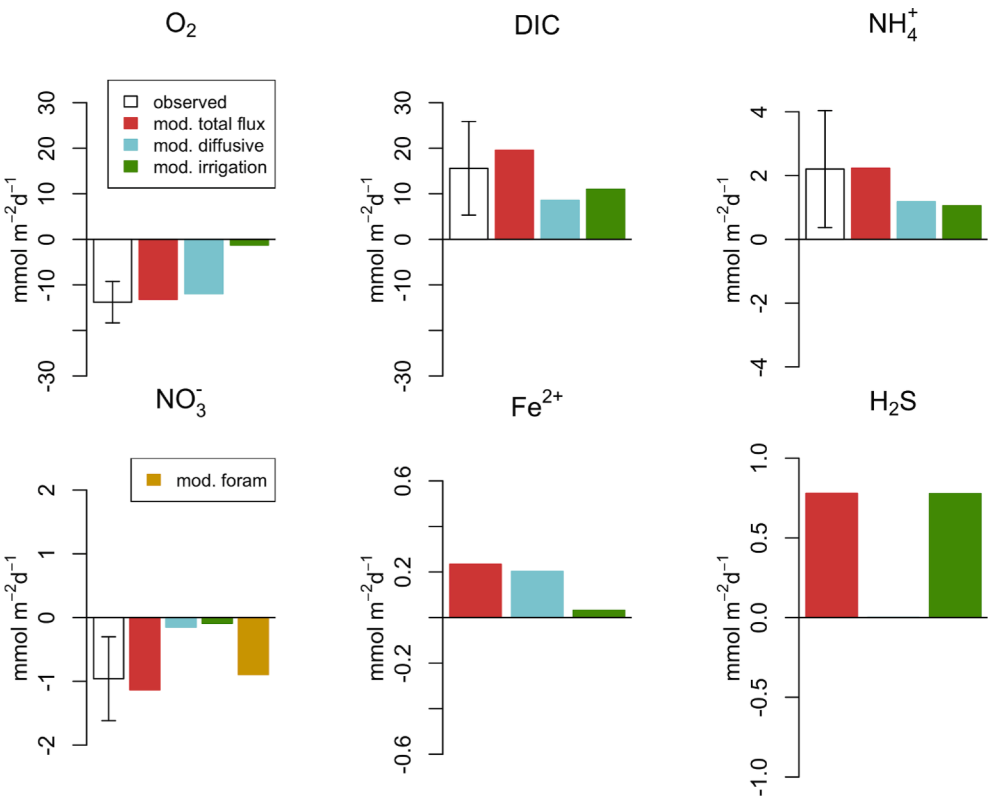

Fig. 3. Modeled and measured benthic solute fluxes. Measured mean benthic flux (Table 1) is shown by the white bars. The red bars represent the model predicted steady state flux, which is the sum of diffusive (blue) and bioirrigation (green) fluxes. The nitrate flux shows additional contribution from foraminiferal uptake. Fe(II) and H_2S fluxes were not measured.

Table 2
Organic carbon and nitrogen mineralization rate (nmol cm^{-3} d^{-1}) determined from the anoxic incubations.

Depth (cm)	Nov 2020			May 2021		
	C_{min}	N_{min}	C_{min}:N_{min}	C_{min}	N_{min}	C_{min}:N_{min}
0–2	409.1 ± 42.4	51.1 ± 7.1	8	237.9 ± 25.4	36.8 ± 6.3	6.5
2–4	143.9 ± 19.1	24.5 ± 1.3	5.9	112.4 ± 15	18.2 ± 1.8	6.2
8–10	61.3 ± 8.4	6.9 ± 0.2	8.8	54.5 ± 7.2	9.8 ± 0.9	5.6
16–18	73.2 ± 28.7	4.6 ± 0.6	16	48 ± 20	8.2 ± 1.2	5.9

sediment, although bioirrigation could also be performed by other organisms that possibly were present. Bioirrigation contributed nearly 50% of the benthic flux of NH_4^+ and DIC (Fig. 3). On the other hand, benthic oxygen uptake was dominated by molecular diffusion, with bioirrigation accounting for only ~10%. For nitrate uptake, both diffusion and bioirrigation played a minor role (~14% and ~8% respectively). Nitrate uptake was instead dominated by foraminifera (~78%) (Fig. 3) and channeled into foraminiferal denitrification. The model-predicted foraminiferal denitrification rate of 0.9 mmol m^{-2} d^{-1} was within the same order of magnitude as experimentally estimated by upscaling individual rates from living foraminiferal abundances (see Section 3.5 and 4.3).

4. Discussion

4.1. Organic matter turnover and benthic fluxes

The depositional organic carbon flux measured in BB in the 1970s ranged from 17.2 to 21 mmol C m^{-2} d^{-1} (Hargrave and Taguchi, 1976, 1978). This is in good agreement with our model estimate of 25.2 mmol C m^{-2} d^{-1}. Our model estimated flux falls within the ^{234}Th estimated flux of 70±70 mmol C m^{-2} d^{-1} from BB (Black et al., 2023). More data are required to determine whether the apparent 20–40% increase in carbon flux in our model compared to the 1970s forms part of a long-term trend due to eutrophication or whether it represents normal variation around the annual mean. The former could be possible due to urban population growth and increasing sewage outfall leading to eutrophication, as nutrients from the outflow are not removed before discharge into Halifax Harbour. The depositional flux of organic carbon in BB sediment is higher than some in Norwegian fjords (2.4–4.3 mmol C m^{-2} d^{-1}) (Lalande et al., 2020), while similar to others (e.g., Fanafjorden, 21.9 – 24.4 mmol C m^{-2} d^{-1}) (Wassmann, 1984) and lower than turbid river-fed fjords (26.5 – 36.8 mmol C m^{-2} d^{-1}) (Hage et al., 2022). The model further revealed a carbon burial rate (i.e., rate of C-sequestration at the bottom of the sediment cores) of 5.6 mmol C m^{-2} d^{-1} suggesting that the organic C burial efficiency in BB sediment is 23%. This is similar to the carbon burial of 6 mmol C m^{-2} d^{-1} recently estimated for BB (Black et al., 2023). The carbon burial efficiency in BB is greater than in some high arctic and temperate fjord and shelf areas (5–20%) (Kuliński et al., 2014) while similar to others (Smith et al., 2015; Faust and Knies, 2019; Lalande et al., 2020). BB thus appears to be an important site of organic carbon sequestration.

Organic carbon mineralization in BB was dominated by sulfate reduction (71%) (Fig. 6A) in agreement with other fine-grained coastal sediments (Jørgensen and Kasten, 2006). Aerobic respiration (11%) was the second most important pathway for OM degradation. Total

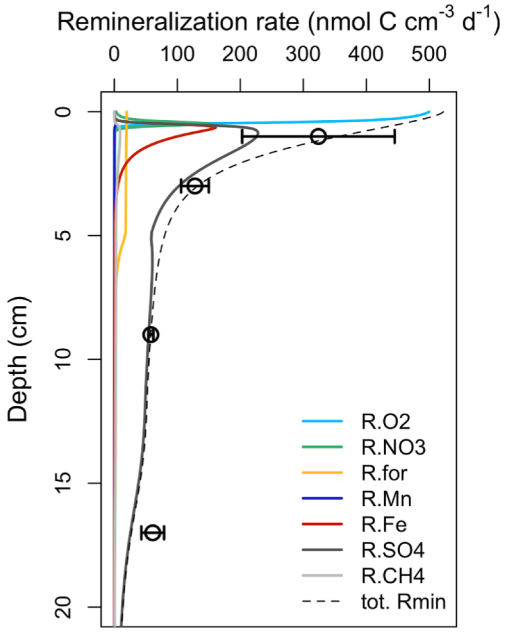

Fig. 4. Organic carbon remineralization rate at different depths in the sediment. The open circles denote the measured average organic carbon remineralization rate determined from the anoxic incubations. Simulated organic matter remineralization rates by different electron acceptors are shown as solid lines (Table S2). The dashed line denotes the sum of all the modeled remineralizations pathways (tot. Rmin). Note: 'R.for' in the legend indicates remineralization by foraminiferal denitrification.

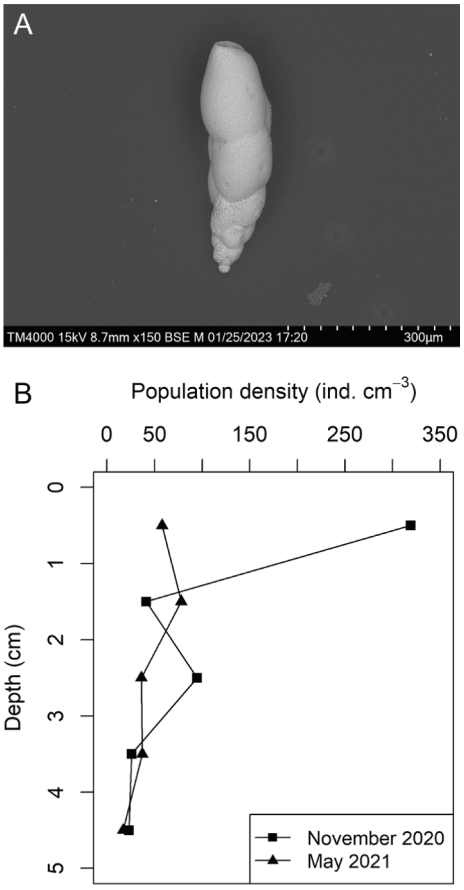

Fig. 5. (A) Scanning electron microscopic (SEM) image of foraminifera, *Stainforthia fusiformis*, the most abundant benthic foraminifera at the deepest part of Bedford Basin, capable of storing intracellular nitrate at high concentrations. (B) Population density of *Stainforthia fusiformis*, in the > 63 µm fraction of top 5 cm of sediment.

denitrification contributed by canonical (2%) and foraminiferal (6%) denitrification accounted for the third followed by iron oxide reduction (7%). The simulated benthic DIC and NH_4^+ flux was 19.6 and 2.2 mmol m^{-2} d^{-1}, respectively, with bioirrigation accounting for ~50% of the total flux (Fig. 3). However, bioirrigation contributed only 10% of total benthic oxygen uptake (Fig. 3) indicating total oxygen uptake is dominated by diffusion in BB (Rakshit et al., 2023). The overestimation of the oxygen penetration depth in our model compared to observations could be due to the differences of in-situ versus ex-situ measurements of oxygen concentrations, whereby in-situ penetration depths tend to be larger (Jørgensen et al., 2022). Another possible reason could be that in our model we considered three pools of OM and constrained the OM decay constants with observed remineralization rates in two-centimeter sections of the core as obtained from anoxic incubations. This probably did not adequately capture the very reactive fraction of OM at the sediment surface, which could consume oxygen more rapidly than our model simulates.

The modeled nitrogen budget for BB sediment (Fig. 6B) indicates that the majority (96%) of NH_4^+ produced by ammonification is lost from the sediment via diffusion and bioirrigation while a minor portion undergoes nitrification. The calculated burial of the deposited organic nitrogen was 0.5 mmol N m^{-2} d^{-1}, which is within the range of global N burial rates of 0.002–1.8 mmol N m^{-2} d^{-1} compiled from various ecosystems (Koziorowska et al., 2018). Considering the total N budget, the BB sediment acts as a net sink of N, removing 1.8 mmol m^{-2} d^{-1} of fixed N by denitrification and burial. The model suggests that the total denitrification is 1.3 mmol N m^{-2} d^{-1}, where 0.9 mmol m^{-2} d^{-1} (70%) was carried out via foraminiferal denitrification, while canonical denitrification accounted for 30% of total denitrification. The nitrate influx observed in BB sediment (1.1 mmol m^{-2} d^{-1}) was higher than in Eckernförde Bay, a similar seasonally hypoxic basin in the western Baltic Sea (Dale et al., 2011) where a nitrate influx of 0.35±0.12 mmol m^{-2} d^{-1} was measured in winter, out of which 75% was ascribed to DNRA

Table 3
Foraminifera abundances for the dominant species present in the 0–5 cm sediment interval at Bedford Basin Compass Buoy station. See the text for calculation of total foraminiferal denitrification.

	Abundance (ind. cm^{-2})	Intracellular storage (mM)	Total foraminiferal denitrification rate (mmol N m^{-2} d^{-1})
November 2020			
Stainforthia fusiformis	474	n/a	0.33
Elphidium bartletti	21	n/a	n/a
Other species	1	n/a	n/a
May 2021			
Stainforthia fusiformis	201	n/a	0.14
Elphidium bartletti	31	n/a	n/a
Other species	2	n/a	n/a
March 2022			
Stainforthia fusiformis	n/a	107 ± 43	n/a

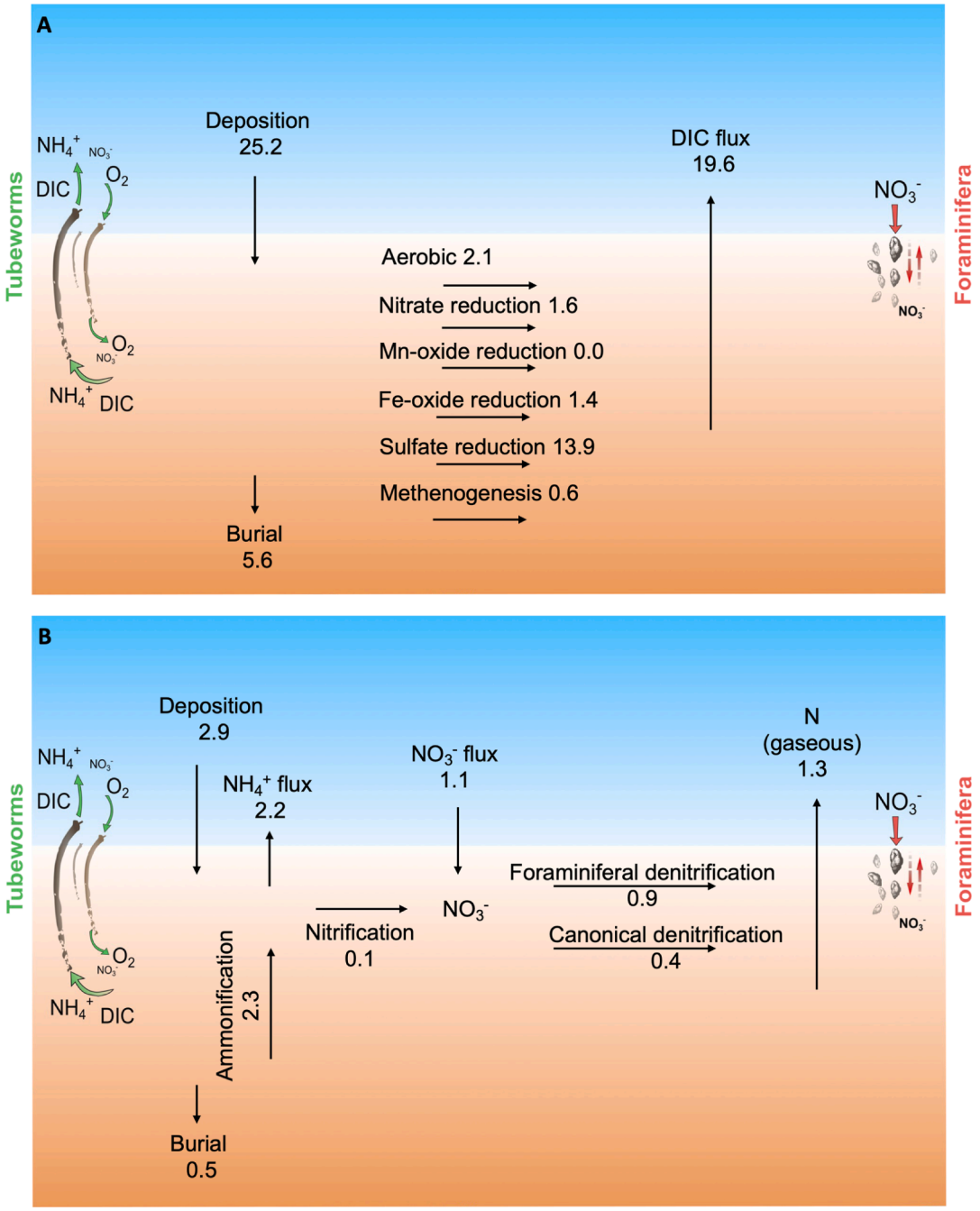

Fig. 6. Benthic (A) carbon and (B) nitrogen budget of Bedford Basin. Values are given in the unit of mmol C m^{-2} d^{-1} and mmol N m^{-2} d^{-1} for carbon and nitrogen respectively. Additionally, schematic diagram of the actions of tubeworms and foraminifera relevant to Bedford Basin sediment are shown. (The figure is not to scale).

while 25% was ascribed to canonical denitrification. However, the NH_4^+ efflux of 1.74 ± 0.15 mmol m^{-2} d^{-1} at this site was similar to BB. In a previous work from BB, Burt et al. (2013) calculated benthic fluxes of nitrate, DIC and oxygen from the eddy diffusion estimates from ^{224}Ra measurements in the water column. Their DIC and oxygen fluxes were generally higher than our model estimates and the calculated nitrate flux was in the opposite direction (i.e., the sediment was a source of nitrate in their work) than observed in the current study. It should be noted that in their work, they assumed negligible water column remineralization and nitrification, and attributed all sources and sinks to the sediment. On the contrary, later works found that bottom water nitrification is a major feature in BB (Haas et al., 2021), and that water column respiration could be responsible for 80% of oxygen consumption in the basin while benthic respiration contributed 20% to the total oxygen consumption below the sill depth at BB Compass Buoy site (Rakshit et al., 2023).

Our modeled dissolved iron flux of 0.2 mmol Fe m^{-2} d^{-1} from the sediment to the overlying water could be amongst the highest reported rates of dissolved Fe release (Dale et al., 2015). However, this should be confirmed through further empirical measurements. In the BB water column, particulate iron concentrations and Fe/Al ratios increase with water depth (Hargrave, 1989) which could be due to the reoxidation of benthic-derived dissolved iron in the water column. We found that H_2S barely accumulated in the upper 20 cm of the sediment even though sulfate reduction accounts for 71% of OM degradation and becomes the dominant OM remineralization pathway below 1.2 cm (Fig. 4). Interestingly, our model calculated oxygen budget (Fig. 7) indicates that the majority of benthic oxygen consumption can be attributed to iron

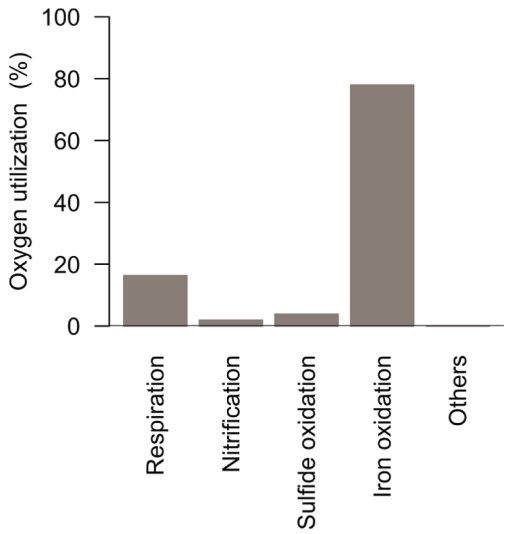

Fig. 7. Oxygen budget in Bedford Basin sediment showing percent oxygen consumption via different biogeochemical reactions as revealed by the model.

oxidation, whereas sulfide oxidation accounts for a minor fraction. This result is to be expected because the oxygen penetration depth in sediment is ~1 mm, such that majority of the H_2S produced in the sediment is rapidly precipitated into iron-sulfide/pyrite mineral phases before it can diffuse into the oxic surface layer. Indeed, consideration of the total Fe(III) deposition flux and Fe(III) required to support remineralization of 1.4 mmol C m^{-2} d^{-1} (Fig. 6A) suggest that deposited iron must go through three cycles of oxidation–reduction before ultimate burial as pyrite. This is driven by active shuttling of reduced and oxidized forms of iron in top few centimeters of sediment through different transport pathways (Van Cappellen and Wang, 1996). This is similar to the rapid metal cycling at the Skagerrak induced by bioturbation where deposited Fe and Mn is oxidized and reduced 100–300 times before being finally buried (Canfield et al., 1993).

The limitation of the current model approach lies in the use of a steady state assumption to simulate benthic biogeochemistry in a basin with distinct seasonality. The bottom water conditions change from oxic to severely hypoxic in an annual cycle along with seasonal changes in organic matter flux and bottom water concentrations of nutrients (Haas et al., 2021; Rakshit et al., 2023). Although the mean biogeochemical data from seven field campaigns spanning three years were used to constrain the model, a transient model would provide more detailed understanding of biogeochemical processes incorporating the seasonal variations (Soetaert et al., 1996b; Dale et al., 2017). Nevertheless, the steady state model is able to elucidate coupled biogeochemical processes and forms a solid first approach in studying a complex natural system (Soetaert et al., 1996a; Bohlen et al., 2011; Dale et al., 2016). The findings from this model help to identify key parameters and the dominant biogeochemical drivers for further development of seasonal models.

4.2. *The impact of tubeworms on sediment geochemistry*

The tubeworms, *Spiochaetopterus* sp., predominant in BB sediment (Hargrave 1989; Fader and Miller 2008; This study) are polychaetes of the family Chaetopteridae and are a common species along the North Atlantic coast (Barnes, 1964). They are typically 3–6 cm in length and construct vertical tubes up to 30 to 50 cm by secreting chitin-like material (Barnes 1964, this study). Under high flow regimes in the bottom water, they carry out suspension feeding, whereas deposit feeding predominates at lower flow regimes (Turner and Miller, 1991). They egest waste as elongated fecal pellets shaped like a grain of rice and ejected through the upper opening of the tube (Barnes, 1964). This probably explains the fecal pellets we observed on the collected sediment cores. The worms move vertically through the tubes frequently for the purpose of feeding, cleaning, or constructing new segments to their tube. Their membranelles beat continually ensuring continuous water circulation in the tube which is essential for their survival (Barnes, 1964). Moreover, ambient bottom currents can induce passive flushing of relict tubes of *Spiochaetopterus* sp. (Munksby et al., 2002). Therefore, the activity of tubeworm-induced bioirrigation can have a major influence on the biogeochemistry of the sediment.

Bioirrigation intensity is traditionally measured from incubated sediment cores using an inert tracer such as bromide. However, this technique has been questioned, especially for ex-situ measurements

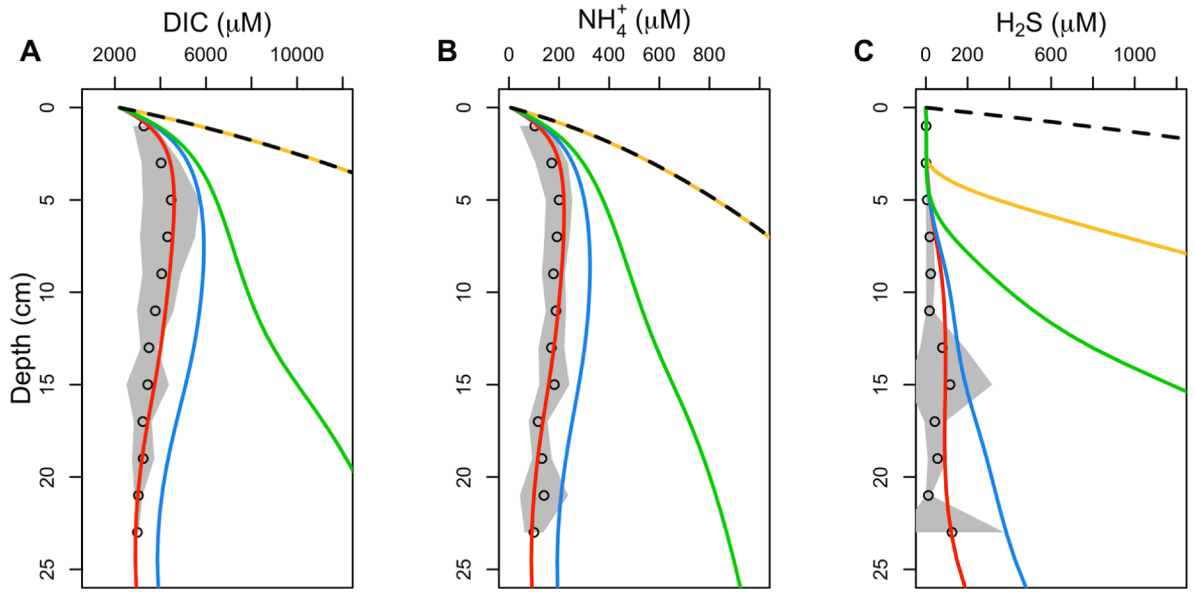

Fig. 8. Model experiment with varying bioirrigation. The symbols and gray shading are measured seasonal mean concentrations and standard deviation respectively. The solid red lines are identical to Fig. 2 representing optimized model simulation. Other model curves correspond to different model simulations as explained in section 4.2 – (i) blue line: bioirrigation coefficient reduced by a factor of 2, (ii) green line: bioirrigation coefficient and depth of bioirrigation reduced by a factor of 2, (iii) yellow line: turned off bioirrigation and (iv) dashed black line: turned off bioirrigation and lowered the bottom water oxygen to 10 μM.

Table 4
Literature data on benthic foraminiferal denitrification from other sites compared to Bedford Basin. OMZ = oxygen minimum zone.

Study area	Rate of foraminiferal denitrification (mmol N m^{-2} d^{-1})	% of total denitrification	Method*	Environment and water depth (m)	Reference
Bedford Basin	0.14–0.9	25–70 %	e, m	Seasonally hypoxic, 70 m	*This study*
Peruvian OMZ	1.4–1.5	87–90 %	m	Sediment below OMZ, 309–409 m	(Dale et al., 2016)
Skagerrak	0.72	70 %	e	Oxic sediments, 210 m	(Piña-Ochoa et al., 2010)
Bay of Biscay canyon	0.064	84 %	e	Canyon, oxic, 453 m	(Piña-Ochoa et al., 2010)
Chilean OMZ	0.173	70 %	e	Sediment below OMZ, 88 m	(Piña-Ochoa et al., 2010)
Arabian Sea OMZ	0.078	9–15 %	e	Sediment below OMZ, 200–1200 m	(Piña-Ochoa et al., 2010)
Tagus Prodelta, estuary	0.072–0.240	8–50 %	e	Estuary	(Piña-Ochoa et al., 2010)
Sagami Bay	0.05	4 %	e,l	Hypoxic, 1450 m	(Glud et al., 2009)
Peruvian OMZ	0.013–1.32	2–100 %	e	Sediment below OMZ, 80–700 m	(Glock et al., 2013)
Yellow Sea and East China Sea	0.016–0.088	24–61 %	e	Shelf sediment, oxic, 63–97 m	(Xu et al., 2017)
Gullmar Fjord	0.062–0.133	47–100 %	e,l	Fjord, oxic site, 50 m	(Choquel et al., 2021)
Bering Sea	0.0001–0.002	0.3–6 %	e	Shelf sediments, oxic to hypoxic, 103–1536 m	(Langlet et al., 2020)

* e = empirical, m = modeling, l = measured in lab.

where the activity of irrigating fauna is likely to be affected during sediment core handling (Kristensen et al., 2018). Therefore, alternative techniques, such as using pore water profiles of NH_4^+ or DIC have been suggested to be used to constrain bioirrigation profiles, as we have used in this study (Kristensen et al., 2018). We found that constant deep bioirrigation down to 30 cm depth was required to fit our model to the data (Figure S7). However, we do not rule out even deeper depths of active bioirrigation as we lack data showing a gradual increase of pore water concentrations of NH_4^+ and DIC at the base of the bioirrigation zone (Aller, 1980). The application of a constant bioirrigation rate from surface to deep layers based on porewater profiles of NH_4^+ and DIC implies that the bioirrigation rate is well constrained at depth. Nevertheless, higher bioirrigation at shallow depths cannot be ruled out, as near the sediment water interface the difference between the NH_4^+ and DIC concentrations in the porewater and the bottom water is small. Hence a change in α there does not affect the flux of these chemicals as much therefore it is probably not very well constrained there. Indeed, a model experiment (not shown) increasing the bioirrigation by a factor of two did not significantly change the porewater fit of NH_4^+ and DIC in the top 2 cm, but below this depth the concentrations were underestimated. An increase in α near the surface impacted O_2 fluxes by increasing the bioirrigation driven oxygen uptake because the O_2 penetration is only a few millimeters.

To understand the controls of bioirrigation on the subsurface geochemical distribution at BB, we performed a number of model sensitivity experiments (Fig. 8). These include (i) reducing the bioirrigation coefficient by a factor of two, (ii) as (i) with a further reduction of the depth of active bioirrigation by a factor of two (i.e., the bioirrigation zone was 15 instead of 30 cm thick), (iii) turning off bioirrigation, and (iv) turning off bioirrigation in addition to lowering the bottom water oxygen to 10 μM to represent oxygen deficient conditions in bottom waters.

Lowering the bioirrigation coefficient by a factor of two (scenario (i)) retained the shape of the depth profiles for DIC, NH_4^+ although their concentration increased and H_2S started to accumulate towards the bottom of the simulated core (blue line in Fig. 8). When we further reduced the depth of constant bioirrigation to 15 cm (scenario (ii)), DIC, NH_4^+ and H_2S concentration increased significantly, suggesting that the bioirrigation depth has a more important control on subsurface solute concentrations than the flushing rate (green line in Fig. 8). Turning off bioirrigation (scenario (iii)) led to a further shoaling of DIC, NH_4^+ and accumulation of H_2S below 3 cm depth (yellow line in Fig. 8). Further lowering of bottom water oxygen to 10 μM (scenario (iv)) made little difference to DIC and NH_4^+ concentrations from the previous case, although H_2S started to accumulate near the surface sediment and H_2S diffused out to the bottom water (black dashed line in Fig. 8), indicating a reduction in iron redox cycling. The model experiments therefore indicate that bioirrigation exerts strong control on the distribution of pore water solutes. The H_2S oxidation in the sediment is primarily controlled by iron-redox shuttling by bioturbation and is important for maintaining the decimeter scale suboxic zone in BB sediment under normal oxic conditions. We hypothesize that tubeworm mortality or disappearance due to ecosystem shifts would result in a shallowing of the suboxic zone, although bioturbation and iron redox cycling would help to maintain sulfide-free porewaters below the sediment surface.

The ecological benefit of the tubeworms to construct tubes that are longer than 30 cm is not clear. The presence of living worms down to 30 cm indicates that they spend considerable amounts of time towards the bottom end of the tube. The availability of fresh organic matter is likely to be higher towards the upper end of the tube. Therefore, the apparent indication of them spending time at the bottom suggests some form of benefit they receive which could include predator avoidance. Although not yet observed for *Spiochaetopterus* sp. to the best of our knowledge, mutualism in tubeworms with symbiont sulfide oxidizing bacteria has been documented in a variety of habitats including hydrothermal vents, cold seeps, and fjords (Stewart et al., 2005). Thus, it is worth investigating if there exists a symbiosis between microbial consortia and *Spiochaetopterus* sp. which might contribute to sulfide oxidation and detoxification within the tubes (Cordes et al., 2005; Sato and Sasaki, 2021). Future studies could focus on quantitative estimates of benthic macrofauna and their spatiotemporal abundance, identification, combined with genomics and modeling to better understand their ecological role.

4.3. Significance of foraminiferal denitrification

Denitrifying foraminifera probably acquired the genes necessary for denitrification from bacteria since foraminiferal denitrification has been suggested to have an ancient origin (Woehle et al., 2022). Foraminifera are motile and use their pseudopodial network for locomotion. They can access nitrate from the surface sediment through vacuoles and pores and can migrate to deeper layers to escape predation or actively seek out fresh organic matter. Thus, they have a competitive advantage over non-motile bacteria (Fig. 4). The benthic foraminifer, *S. fusiformis*,

contributing to foraminiferal denitrification in BB, appears to be a relatively recent inhabitant of the basin as their abundance has increased largely after the 1970s (Scott, 2005). It is a low oxygen tolerant species (Nordberg et al., 2000) indicating that oxygen levels may have deteriorated over the last few decades. The foraminiferal denitrification rate estimated from the living abundances of *S. fusiformis* (Table 3) and the individual denitrification rate of *Stainforthia* sp. (70 pmol N ind^{-1} d^{-1}) from Piña-Ochoa et al. (2010) is 0.14–0.33 mmol m^{-2} d^{-1}, which is lower than the modeled foraminiferal denitrification rate of 0.9 mmol m^{-2} d^{-1}. One reason for this discrepancy might be related to the lack of measurements of denitrification rates for *S. fusiformis*. The denitrification rate published for *Stainforthia* sp. (Pina-Ochoa et al., 2010) is one of the lowest species-specific denitrification rates for foraminifera that has yet been measured (Glock, 2023). It is possible that the average denitrification rate for *S. fusiformis* is higher. Previous works have also indicated that meiofaunal and foraminiferal bioturbation and bioirrigation can stimulate benthic denitrification which needs to be investigated further (Bonaglia et al., 2014; Langlet et al., 2023).

Another factor is that the model assumes steady state, meaning that nitrate uptake by foraminifera is balanced by foraminiferal denitrification. Measured NO_3^- uptake rates of benthic foraminifera can be up to five times higher than their rate of denitrification (Koho et al., 2011). This difference may reflect temporary decoupling between uptake and denitrification which would not be captured in our steady state model. Our measurements of the intracellular NO_3^- storage in *S. fusiformis* reveal that there is a rich reservoir of NO_3^- stored in foraminifera that sometimes exceed the pore water NO_3^- content. If we account for the likely higher uptake rate and experimentally determined foraminiferal denitrification rate, then the foraminiferal NO_3^- uptake becomes similar to the total foraminiferal denitrification rate predicted by the model. The extra nitrate uptake must however be denitrified if the system is to remain balanced in the longer term. This consideration indicates that the rate estimated from foraminiferal abundance is probably the lowest denitrification rate in the BB sediment and the model estimated rate is towards the upper bound of this rate. The seasonal denitrification rates may lie within this range. Nevertheless, the rate of foraminiferal denitrification estimated in BB lies towards the upper end of the global reports of foraminiferal denitrification (Table 4), suggesting they may increase denitrification in places faced by increased hypoxia and contribute significantly to N-loss from the system mitigating eutrophication.

This perception, however, may not be exclusively true as non-indigenous species of denitrifying foraminifera in Gullmar fjord were recently found to dominate benthic denitrification in oxic sediment, whereas in sediments below hypoxic water they contributed <5% to denitrification (Choquel et al., 2021). Prolonged hypoxia or anoxia could cause their activity to reduce as it has been suggested that some denitrifying foraminifera are probably facultative anaerobes and respire nitrate to maintain basic survival functions in the absence of oxygen but require oxygen for energy intensive functions such as growth or reproduction (Piña-Ochoa et al., 2010). An earlier mesocosm study (Alve and Bernhard, 1995) found that under low oxygen condition foraminifera can migrate to polychaete tubes to fulfill their oxygen needs; it seems plausible that such interactions could be present in BB and should be investigated in future. Interestingly, laboratory experiments found that while most denitrifying foraminifera and their bacterial consortia can perform complete denitrification to N_2 gas (Woehle et al., 2022), some foraminifera such as *Bolivina plicata, Stainforthia sp*. etc. may lack nitrous oxide reductase and produce nitrous oxide (N_2O) as the end product which makes them a source of this potent greenhouse gas (Piña-Ochoa et al., 2010). Therefore, the colonization of species such as *Stainforthia fusiformis* in low oxygen environments like BB as studied here, or in other fjords e.g., Gullmar fjord (Nordberg et al., 2000; Polovodova Asteman and Nordberg, 2013), generates concerns on its possible impact on global warming with changing environmental conditions. Although the produced N_2O could be utilized by other denitrifying bacteria in the system, further study is nonetheless needed to ascertain the roles of foraminiferal denitrification in the marine greenhouse gas budget.

To the best of our knowledge, this work is the first study describing the evidence of foraminiferal denitrification together with quantitative estimation from observations and diagenetic modeling. We report the first evidence of benthic foraminiferal denitrification in the western Atlantic coastal sediments, which combined with observations from a variety of other marine sediment settings suggest this phenomenon may be widespread (Glock, 2023; and Table 4). Furthermore, in several of the sites where this has been studied, including our work, foraminifera can be responsible for a majority of the total benthic denitrification (Table 4). This suggests eukaryotic denitrification may be an important pathway of N-loss from marine sediments, which is in contrast to the traditional view that this is primarily mediated by prokaryotic microbes. Since their first identification (Risgaard-Petersen et al., 2006), several denitrifying foraminifera have been identified in various ecosystems, many of which appeared to thrive in low oxygen environments (Glock, 2023). As coastal hypoxia has expanded during the last few decades (Breitburg et al., 2018), foraminifera capable of denitrification may become more widely distributed and, thus, increasingly important for benthic nitrogen cycling.

5. Conclusions

In this work, we studied early diagenesis in the seasonally hypoxic Bedford Basin; a natural laboratory for studying oxygen sensitive biogeochemical processes in the coastal ocean. We employed direct measurements of benthic fluxes and porewater profiles of oxygen, DIC, nutrients and major redox species. An empirical reaction-transport model was used to study the yearly averaged biogeochemical cycling in the sediments. We conclude that long tubeworms led to inverse pore water profiles of NH_4^+ and DIC and contributed to nearly half of the NH_4^+ and DIC efflux from sediment. Together with bioturbation and intense iron turnover, tubeworms help to prevent accumulation of hydrogen sulfide in upper few decimeters of the sediment despite an oxygen penetration depth of only a few millimeters. Foraminiferal denitrification was required in the model to reproduce the observed nitrate influx. Experiments and modeling indicated that the foraminiferal denitrification rate in BB is among the highest globally and could contribute up to 70% of the total denitrification in BB, indicating the potential importance of benthic foraminiferal denitrification in seasonally hypoxic environments. The present study examined the influence of these benthic fauna on the annually averaged early diagenetic processes. Future studies should focus on studying the seasonal patterns of these organisms and diagenetic processes in response to transient hypoxia.

CRediT authorship contribution statement

Subhadeep Rakshit: Writing – review & editing, Writing – original draft, Visualization, Validation, Software, Resources, Project administration, Methodology, Investigation, Funding acquisition, Formal analysis, Data curation, Conceptualization. **Nicolaas Glock:** Writing – review & editing, Methodology, Investigation, Funding acquisition, Formal analysis, Data curation. **Andrew W. Dale:** Writing – review & editing, Supervision, Resources, Investigation. **Maria M.L. Armstrong:** Writing – review & editing, Resources, Project administration, Methodology, Formal analysis, Data curation. **Florian Scholz:** Writing – review & editing, Methodology, Investigation, Formal analysis, Data curation. **Andrè Mutzberg:** Methodology, Formal analysis. **Christopher K. Algar:** Writing – review & editing, Validation, Supervision, Resources, Project administration, Methodology, Investigation, Funding acquisition, Formal analysis, Data curation, Conceptualization.

Data availability

Data are available through FigShare at https://doi.org/10.6084/m9.

figshare.27074893. The model code is available through Zenodo at https://doi.org/10.5281/zenodo.13893493.

Declaration of competing interest

The authors declare that they have no known competing financial interests or personal relationships that could have appeared to influence the work reported in this paper.

Acknowledgement

The research was supported through an NSERC Discovery Grant, and the Ocean Frontier Institute. The Transatlantic Ocean System Science and Technology (TOSST) Graduate School and the Nova Scotia Graduate Scholarship Program provided PhD stipend support to SR. We would like to thank the boat captains of Connors Diving for helping during sampling. NG would like to thank the Deutsche Forschungsgemeinschaft (DFG) for funding through grants GL 999/3-1 and GL 999/4-1. Additional funding was provided by the Ocean Frontiers Institute (OFI) to N. G. through the Visiting Fellowship Program (2020). We would also like to thank the associate editor, along with Hal Bradbury, and two other anonymous reviewers for their constructive comments.

Appendix A. Supplementary material

The supplementary material consists of supplementary figure S1-S7, which includes data and image from sediment cores, individual porewater profiles, data from anoxic incubation experiment and some model results. The supplementary tables S1-S5 include the model state variables, model equations, boundary conditions and rate constants. The supplementary table S6 contains foraminifera count data. Supplementary material to this article can be found online at https://doi.org/10.1016/j.gca.2024.10.010.

References

Aller, R.C., 1980. Quantifying solute distributions in the bioturbated zone of marine sediments by defining an average microenvironment. Geochim. Cosmochim. Acta 44, 1955–1965.
Alve, E., Bernhard, J.M., 1995. Vertical migratory response of benthic foraminifera to controlled oxygen concentrations in an experimental mesocosm. Mar. Ecol. Prog. Ser. 116, 137–151.
Barnes, R.D., 1964. Tube-building and feeding in the chaetopterid polychaete, Spiochaetopterus oculatus. Biol. Bull. 127, 397–412.
Berg, P., Rysgaard, S., Thamdrup, B., 2003. Dynamic Modeling of Early Diagenesis and Nutrient Cycling. A Case Study in an Artic Marine Sediment. Am. J. Sci. 303, 905–955.
Berner, R.A., 1980. Early Diagenesis: A Theoretical Approach. Princeton University Press.
Bernhard, J.M., Casciotti, K.L., McIlvin, M.R., Beaudoin, D.J., Visscher, P.T., Edgcomb, V. P., 2012. Potential importance of physiologically diverse benthic foraminifera in sedimentary nitrate storage and respiration. J. Geophys. Res. Biogeosci. 117, n/a-n/a.
Black, E.E., Algar, C.K., Armstrong, M., Kienast, S.S., 2023. Insights into constraining coastal carbon export from radioisotopes. Front. Mar. Sci. 10, 1–20.
Bohlen, L., Dale, A.W., Sommer, S., Mosch, T., Hensen, C., Noffke, A., Scholz, F., Wallmann, K., 2011. Benthic nitrogen cycling traversing the Peruvian oxygen minimum zone. Geochim. Cosmochim. Acta 75, 6094–6111.
Bohlen, L., Dale, A.W., Wallmann, K., 2012. Simple transfer functions for calculating benthic fixed nitrogen losses and C:N: P regeneration ratios in global biogeochemical models. Global Biogeochem. Cycles 26.
Bonaglia, S., Nascimento, F.J.A., Bartoli, M., Klawonn, I., Brüchert, V., 2014. Meiofauna increases bacterial denitrification in marine sediments. Nat. Commun. 5, 5133.
Boudreau, B.P., 1996. The diffusive tortuosity of fine-grained unlithified sediments. Geochim. Cosmochim. Acta 60, 3139–3142.
Boudreau, B.P., 1997. Diagenetic Models and Their Implementation. Springer, Berlin Heidelberg, Berlin, Heidelberg.
Breitburg, D., Levin, L.A., Oschlies, A., Grégoire, M., Chavez, F.P., Conley, D.J., Garçon, V., Gilbert, D., Gutiérrez, D., Isensee, K., Jacinto, G.S., Limburg, K.E., Montes, I., Naqvi, S.W.A., Pitcher, G.C., Rabalais, N.N., Roman, M.R., Rose, K.A., Seibel, B.A., Telszewski, M., Yasuhara, M., Zhang, J., 2018. Declining oxygen in the global ocean and coastal waters. Science (1979) 359, eaam7240.
Burdige, D.J., 2011. Estuarine and Coastal Sediments – Coupled Biogeochemical Cycling. In: Treatise on Estuarine and Coastal Science, Elsevier, pp. 279–316.
Burke, M.J., Gusta, L.V., Quamme, H.A., Weiser, C.J., Li, P.H., 1976. Freezing and Injury in Plants. Annu. Rev. Plant Physiol. 27, 507–528.
Burt, W.J., Thomas, H., Fennel, K., Horne, E., 2013. Sediment-water column fluxes of carbon, oxygen and nutrients in Bedford Basin, Nova Scotia, inferred from 224 Ra measurements. Biogeosciences 10, 53–66.
Canfield, D.E., Raiswell, R., Westrich, J.T., Reaves, C.M., Berner, R.A., 1986. The use of chromium reduction in the analysis of reduced inorganic sulfur in sediments and shales. Chem. Geol. 54, 149–155.
Canfield, D.E., Thamdrup, B., Hansen, J.W., 1993. The anaerobic degradation of organic matter in Danish coastal sediments: Iron reduction, manganese reduction, and sulfate reduction. Geochim. Cosmochim. Acta 57, 3867–3883.
Choquel, C., Geslin, E., Metzger, E., Filipsson, H.L., Risgaard-Petersen, N., Launeau, P., Giraud, M., Jauffrais, T., Jesus, B., Mouret, A., 2021. Denitrification by benthic foraminifera and their contribution to N-loss from a fjord environment. Biogeosciences 18, 327–341.
Cline, J.D., 1969. Spectrophotometric determination of hydrogen sulfide in natural waters. Limnol. Oceanogr. 14, 454–458.
Cordes, E.E., Arthur, M.A., Shea, K., Arvidson, R.S., Fisher, C.R., 2005. Modeling the Mutualistic Interactions between Tubeworms and Microbial Consortia. In: Vrijenhoek, R.C. (Ed.), PLoS Biol 3, e77.
Dale, A.W., Sommer, S., Bohlen, L., Treude, T., Bertics, V.J., Bange, H.W., Pfannkuche, O., Schorp, T., Mattsdotter, M., Wallmann, K., 2011. Rates and regulation of nitrogen cycling in seasonally hypoxic sediments during winter (Boknis Eck, SW Baltic Sea): Sensitivity to environmental variables. Estuar. Coast. Shelf Sci. 95, 14–28.
Dale, A.W., Nickelsen, L., Scholz, F., Hensen, C., Oschlies, A., Wallmann, K., 2015. A revised global estimate of dissolved iron fluxes from marine sediments. Global Biogeochem. Cycles 29, 691–707.
Dale, A.W., Sommer, S., Lomnitz, U., Bourbonnais, A., Wallmann, K., 2016. Biological nitrate transport in sediments on the Peruvian margin mitigates benthic sulfide emissions and drives pelagic N loss during stagnation events. Deep Sea Res 1 Oceanogr Res Pap 112, 123–136.
Dale, A.W., Graco, M., Wallmann, K., 2017. Strong and Dynamic Benthic-Pelagic Coupling and Feedbacks in a Coastal Upwelling System (Peruvian Shelf). Front. Mar. Sci. 4, 1–17.
de Freitas, T.R., Bacalhau, E.T., Disaró, S.T., 2021. Biovolume Method for Foraminiferal Biomass Assessment: Evaluation of Geometric Models and Incorporation of Species Mean Cell Occupancy. J. Foramin. Res. 51, 249–266.
Dowgert, M.F., Steponkus, P.L., 1984. Behavior of the Plasma Membrane of Isolated Protoplasts during a Freeze-Thaw Cycle. Plant Physiol. 75, 1139–1151.
Fader, G.B.J., Miller, R.O., 2008. Surficial geology. Halifax Harbour, Nova Scotia.
Faust, J.C., Knies, J., 2019. Organic Matter Sources in North Atlantic Fjord Sediments. Geochem. Geophys. Geosyst. 20, 2872–2885.
Field, C.B., Behrenfeld, M.J., Randerson, J.T., Falkowski, P., 1998. Primary Production of the Biosphere: Integrating Terrestrial and Oceanic Components. Science 281, 237–240.
Geslin, E., Risgaard-Petersen, N., Lombard, F., Metzger, E., Langlet, D., Jorissen, F., 2011. Oxygen respiration rates of benthic foraminifera as measured with oxygen microsensors. J. Exp. Mar. Biol. Ecol. 396, 108–114.
Giblin, A., Tobias, C., Song, B., Weston, N., Banta, G., Rivera-Monroy, V., 2013. The importance of dissimilatory nitrate reduction to ammonium (DNRA) in the nitrogen cycle of coastal ecosystems. Oceanography 26, 124–131.
Glock, N., 2023. Benthic foraminifera and gromiids from oxygen-depleted environments – survival strategies, biogeochemistry and trophic interactions. Biogeosciences 20, 3423–3447.
Glock, N., Schönfeld, J., Eisenhauer, A., Hensen, C., Mallon, J., Sommer, S., 2013. The role of benthic foraminifera in the benthic nitrogen cycle of the Peruvian oxygen minimum zone. Biogeosciences 10, 4767–4783.
Glock, N., Romero, D., Roy, A.S., Woehle, C., Dale, A.W., Schönfeld, J., Wein, T., Weissenbach, J., Dagan, T., 2020. A hidden sedimentary phosphate pool inside benthic foraminifera from the Peruvian upwelling region might nucleate phosphogenesis. Geochim. Cosmochim. Acta 289, 14–32.
Glud, R.N., Thamdrup, B., Stahl, H., Wenzhoefer, F., Glud, A., Nomaki, H., Oguri, K., Revsbech, N.P., Kitazato, H., 2009. Nitrogen cycling in a deep ocean margin sediment (Sagami Bay, Japan). Limnol. Oceanogr. 54, 723–734.
Haas, S., Robicheau, B.M., Rakshit, S., Tolman, J., Algar, C.K., LaRoche, J., Wallace, D.W. R., 2021. Physical mixing in coastal waters controls and decouples nitrification via biomass dilution. Proc. Natl. Acad. Sci. 118.
Haas, S., Rakshit, S., Kalvelage, T., Buchwald, C., Algar, C.K., Wallace, D.W.R., 2022. Characterization of nitrogen isotope fractionation during nitrification based on a coastal time series. Limnol. Oceanogr. 67, 1714–1731.
Hage, S., Galy, V.V., Cartigny, M.J.B., Heerema, C., Heijnen, M.S., Acikalin, S., Clare, M. A., Giesbrecht, I., Gröcke, D.R., Hendry, A., Hilton, R.G., Hubbard, S.M., Hunt, J.E., Lintern, D.G., McGhee, C., Parsons, D.R., Pope, E.L., Stacey, C.D., Sumner, E.J., Tank, S., Talling, P.J., 2022. Turbidity currents can dictate organic carbon fluxes across river-fed fjords: an example from bute inlet (BC, Canada). J. Geophys. Res. Biogeosci. 127, 1–16.
Hannah, F., Rogerson, R., Laybourn-Parry, J., 1994. Respiration rates and biovolumes of common benthic Foraminifera (Protozoa). J. Mar. Biol. Assoc. U. K. 74, 301–312.
Hardison, A.K., Algar, C.K., Giblin, A.E., Rich, J.J., 2015. Influence of organic carbon and nitrate loading on partitioning between dissimilatory nitrate reduction to ammonium (DNRA) and N2 production. Geochim. Cosmochim. Acta 164, 146–160.
Hargrave, B.T., Taguchi, S., 1976. Sedimentation measurements in Bedford Basin, 1973–74. Tech. Rep. isheries Marine Service Environ. 608, 1–129.
Hargrave, B.T., Taguchi, S., 1978. Origin of Deposited Material Sedimented in a Marine Bay. J. Fish. Res. Board Can. 35, 1604–1613.

Hargrave, B.T., 1989. Investigations of marine environmental quality in Halifax Harbour / Edited by H.B. Nicholls. ed. H. B. Nicholls. Can Tech. Rep. Fish Aquat. Sci. 1693, 1–83.

Hayward, B.W., Le Coze, F., Vachard, D., Gross, O., 2023. World Foraminifera Database. Stainforthia fusiformis (Williamson, 1858). Accessed through: World Register of Marine Species at: https://www.marinespecies.org/aphia.php?p=taxdetails&id=113070 on 2023-04-04.

Hendrix, S.A., Braman, R.S., 1995. Determination of nitrite and nitrate by vanadium(III) reduction with chemiluminescence detection. Methods 7, 91–97.

Hepburn, L.E., Butler, I.B., Boyce, A., Schröder, C., 2020. The use of operationally-defined sequential Fe extraction methods for mineralogical applications: a cautionary tale from Mössbauer spectroscopy. Chem. Geol. 543, 119584.

Jahnke, R.A., Reimers Clare, E., Craven, D.B., 1990. Intensification of recycling of organic matter at the sea floor near ocean margins. Nature 348, 50–54.

Jørgensen, B.B., Kasten, S., 2006. Sulfur Cycling and Methane Oxidation. In Marine Geochemistry Springer-Verlag, Berlin/Heidelberg, pp. 271–309.

Jørgensen, B.B., Wenzhöfer, F., Egger, M., Glud, R.N., 2022. Sediment oxygen consumption: Role in the global marine carbon cycle. Earth Sci. Rev. 228, 103987.

Koho, K.A., Piña-Ochoa, E., Geslin, E., Risgaard-Petersen, N., 2011. Vertical migration, nitrate uptake and denitrification: survival mechanisms of foraminifers (Globobulimina turgida) under low oxygen conditions. FEMS Microbiol. Ecol. 75, 273–283.

Koziorowska, K., Kuliński, K., Pempkowiak, J., 2018. Deposition, return flux, and burial rates of nitrogen and phosphorus in the sediments of two high-Arctic fjords. Oceanologia 60, 431–445.

Kristensen, E., Røy, H., Debrabant, K., Valdemarsen, T., 2018. Carbon oxidation and bioirrigation in sediments along a Skagerrak-Kattegat-Belt Sea depth transect. Mar. Ecol. Prog. Ser. 604, 33–50.

Kuliński, K., Kędra, M., Legeżyńska, J., Gluchowska, M., Zaborska, A., 2014. Particulate organic matter sinks and sources in high Arctic fjord. J. Mar. Syst. 139, 27–37.

Lalande, C., Dunlop, K., Renaud, P.E., Nadaï, G., Sweetman, A.K., 2020. Seasonal variations in downward particle fluxes in Norwegian fjords. Estuar. Coast. Shelf Sci. 241, 106811.

Langlet, D., Bouchet, V.M.P., Riso, R., Matsui, Y., Suga, H., Fujiwara, Y., Nomaki, H., 2020. Foraminiferal Ecology and Role in Nitrogen Benthic Cycle in the Hypoxic Southeastern Bering Sea. Front. Mar. Sci. 7.

Langlet, D., Mermillod-Blondin, F., Deldicq, N., Bauville, A., Duong, G., Konecny, L., Hugoni, M., Denis, L., Bouchet, V.M.P., 2023. Single-celled bioturbators: benthic foraminifera mediate oxygen penetration and prokaryotic diversity in intertidal sediment. Biogeosciences 20, 4875–4891.

Lessin, G., Artioli, Y., Almroth-Rosell, E., Blackford, J.C., Dale, A.W., Glud, R.N., Middelburg, J.J., Pastres, R., Queirós, A.M., Rabouille, C., Regnier, P., Soetaert, K., Solidoro, C., Stephens, N., Yakushev, E., 2018. Modelling marine sediment biogeochemistry: current knowledge gaps, challenges, and some methodological advice for advancement. Front. Mar. Sci. 5, 1–8.

Li, W.K.W., Dickie, P.M., Spry, J.A., 1998. Plankton Monitoring Programme in the Bedford Basin, 1991- 1997. Canadian Data Report of Fisheries and Aquatic Sciences 1036, vii + 342.

Li, W.K.W., Harrison, W.G., 2008. Propagation of an atmospheric climate signal to phytoplankton in a small marine basin. Limnol. Oceanogr. 53, 1734–1745.

Li, W.K.W., Lewis, M.R., Harrison, W.G., 2010. Multiscalarity of the nutrient-chlorophyll relationship in coastal phytoplankton. Estuar. Coasts 33, 440–447.

Li, W.K.W., 2014. The state of phytoplankton and bacterioplankton at the Compass Buoy Station: Bedford Basin Monitoring Program 1992-2013. Canadian Technical Report of Hydrography and Ocean Sciences 304, xiv + 122.

McGrath, T., Cronin, M., Kerrigan, E., Wallace, D., Gregory, C., Normandeau, C., McGovern, E., 2019. A rare intercomparison of nutrient analysis at sea: lessons learned and recommendations to enhance comparability of open-ocean nutrient data. Earth Syst. Sci. Data 11, 355–374.

Middelburg, J.J., Soetaert, K., Herman, P.M.J., Heip, C.H.R., 1996. Denitrification in marine sediments: A model study. Global Biogeochem. Cycles 10, 661–673.

Munksby, N., Benthien, M., Glud, R.N., 2002. Flow-induced flushing of relict tube structures in the central Skagerrak (Norway). Mar. Biol. 141, 939–945.

Nordberg, K., Gustafsson, M., Krantz, A.-L., 2000. Decreasing oxygen concentrations in the Gullmar Fjord, Sweden, as confirmed by benthic foraminifera, and the possible association with NAO. J. Mar. Syst. 23, 303–316.

Petrie, B., Yeats, P., 1990. Simple Models of the Circulation, Dissolved Metals, Suspended Solids and Nutrients in Halifax Harbour. Water Quality Res. J. 25, 325–350.

Piña-Ochoa, E., Høgslund, S., Geslin, E., Cedhagen, T., Revsbech, N.P., Nielsen, L.P., Schweizer, M., Jorissen, F., Rysgaard, S., Risgaard-Petersen, N., 2010. Widespread occurrence of nitrate storage and denitrification among Foraminifera and Gromiida. PNAS 107, 1148–1153.

Polovodova Asteman, I., Nordberg, K., 2013. Foraminiferal fauna from a deep basin in Gullmar Fjord: The influence of seasonal hypoxia and North Atlantic Oscillation. J. Sea Res. 79, 40–49.

Poulton, S.W., Canfield, D.E., 2005. Development of a sequential extraction procedure for iron: implications for iron partitioning in continentally derived particulates. Chem. Geol. 214, 209–221.

Rakshit, S., Dale, A.W., Wallace, D.W., Algar, C.K., 2023. Sources and sinks of bottom water oxygen in a seasonally hypoxic fjord. Front. Mar. Sci. 10, 655.

Retschko, A.-K., Vosteen, P., Plass, A., Welter, E., Scholz, F., 2023. Comparison of sedimentary iron speciation obtained by sequential extraction and X-ray absorption spectroscopy. Mar. Chem. 252, 104249.

Risgaard-Petersen, N., Langezaal, A.M., Ingvardsen, S., Schmid, M.C., Jetten, M.S.M., Op den Camp, H.J.M., Derksen, J.W.M., Piña-Ochoa, E., Eriksson, S.P., Peter, N.L., Peter, R.N., Cedhagen, T., van der Zwaan, G.J., 2006. Evidence for complete denitrification in a benthic foraminifer. Nature 443, 93–96.

Sato, M., Sasaki, A., 2021. Evolution and maintenance of mutualism between tubeworms and sulfur-oxidizing bacteria. Am. Nat. 197, 351–365.

Scott, D.B., 2005. Pollution Monitoring in Two North American Estuaries: historical reconstructions using benthic foraminifera. J. Foraminiferal Res. 35, 65–82.

Seitaj, D., Sulu-Gambari, F., Burdorf, L.D.W., Romero-Ramirez, A., Maire, O., Malkin, S. Y., Slomp, C.P., Meysman, F.J.R., 2017. Sedimentary oxygen dynamics in a seasonally hypoxic basin. Limnol. Oceanogr. 62, 452–473.

Shan, S., Sheng, J., Thompson, K.R., Greenberg, D.A., 2011. Simulating the three-dimensional circulation and hydrography of Halifax Harbour using a multi-nested coastal ocean circulation model. Ocean Dyn. 61, 951–976.

Slotznick, S.P., Sperling, E.A., Tosca, N.J., Miller, A.J., Clayton, K.E., van Helmond, N.A. G.M., Slomp, C.P., Swanson-Hysell, N.L., 2020. Unraveling the Mineralogical Complexity of Sediment Iron Speciation Using Sequential Extractions. Geochemistry, Geophysics, Geosystems 21.

Smith, R.W., Bianchi, T.S., Allison, M., Savage, C., Galy, V., 2015. High rates of organic carbon burial in fjord sediments globally. Nat. Geosci. 8, 450–453.

Soetaert, K., Meysman, F., 2012. Reactive transport in aquatic ecosystems: Rapid model prototyping in the open source software R. Environ. Model Softw. 32, 49–60.

Soetaert, K., Herman, P.M.J., Middelburg, J.J., 1996a. A model of early diagenetic processes from the shelf to abyssal depths. Geochim. Cosmochim. Acta 60, 1019–1040.

Soetaert, K., Herman, P.M.J., Middelburg, J.J., 1996b. Dynamic response of deep-sea sediments to seasonal variations: a model. Limnol. Oceanogr. 41, 1651–1668.

Soetaert, K., Middelburg, J.J., Herman, P.M.J., Buis, K., 2000. On the coupling of benthic and pelagic biogeochemical models. Earth Sci. Rev. 51, 173–201.

Soetaert, K., Petzoldt, T., Setzer, R.W., 2010. Solving Differential Equations in R : Package deSolve. J. Stat. Softw. 33, 1–25.

Solórzano, L., 1969. Determination of ammonia in natural waters by the phenolhypochlorite method 1 This research was fully supported by U.S. Atomic Energy Commission Contract No. ATS (11–1) GEN 10, P.A. 20. Limnol. Oceanogr. 14, 799–801.

Stewart, F.J., Newton, I.L.G., Cavanaugh, C.M., 2005. Chemosynthetic endosymbioses: adaptations to oxic–anoxic interfaces. Trends Microbiol. 13, 439–448.

Tromp, T.K., Van Cappellen, P., Key, R.M., 1995. A global model for the early diagenesis of organic carbon and organic phosphorus in marine sediments. Geochim. Cosmochim. Acta 59, 1259–1284.

Turner, E.J., Miller, D.C., 1991. Behavior of a passive suspension-feeder (Spiochaetopterus oculatus (Webster)) under oscillatory flow. J. Exp. Mar. Biol. Ecol. 149, 123–137.

Van Cappellen, P., Wang, Y., 1996. Cycling of iron and manganese in surface sediments; a general theory for the coupled transport and reaction of carbon, oxygen, nitrogen, sulfur, iron, and manganese. Am. J. Sci. 296, 197–243.

Viollier, E., Inglett, P.W., Hunter, K., Roychoudhury, A.N., Van Cappellen, P., 2000. The ferrozine method revisited: Fe(II)/Fe(III) determination in natural waters. Appl. Geochem. 15, 785–790.

Wang, Y., Van Cappellen, P., 1996. A multicomponent reactive transport model of early diagenesis: application to redox cycling in coastal marine sediments. Geochim. Cosmochim. Acta 60, 2993–3014.

Wassmann, P., 1984. Sedimentation and benthic mineralization of organic detritus in a Norwegian fjord. Mar. Biol. 83, 83–94.

Woehle, C., Roy, A.-S., Glock, N., Michels, J., Wein, T., Weissenbach, J., Romero, D., Hiebenthal, C., Gorb, S.N., Schönfeld, J., Dagan, T., 2022. Denitrification in foraminifera has an ancient origin and is complemented by associated bacteria. Proc. Natl. Acad. Sci. 119.

Xu, Z., Liu, S., Xiang, R., Song, G., 2017. Live benthic foraminifera in the Yellow Sea and the East China Sea: vertical distribution, nitrate storage, and potential denitrification. Mar. Ecol. Prog. Ser. 571, 65–81.